Vibration Control of a Suspension System via a Magnetorheological Fluid Damper

by

LAI Chun Yu

A Thesis Submitted in Partial Fulfillment
of the Requirements for the Degree of
Master of Philosophy
in
Mechanical and Automation Engineering

© The Chinese University of Hong Kong

August 2000

The Chinese University of Hong Kong holds the copyright of this thesis. Any person(s) intending to use a part or whole of the materials in the thesis in a proposed publication must seek copyright release from the Dean of the Graduate School.

香港中文大學
圖書館系統
22 JUN 2001
UNIVERSITY
LIBRARY SYSTEM
THE CHINESE UNIVERSITY OF HONG KONG

應用磁流變阻尼器實現單自由度懸掛系統的振動控制

---- 黎俊宇

摘要

半主動控制系統同時具有被動控制系統的可靠性和主動控制系統的可控制特性，而且不需要特別大的能量消耗，因此愈來愈受重視。 磁流變流體可用來設計有效的振動控制執行器，其中磁流變阻尼器就是利用磁流變流體而開發的半主動控制器件，它能產生可控制阻尼力。 本論文的目的是研究採用磁流變阻尼器實現單自由度懸掛系統的振動控制。 在研究中採用了一種描述磁流變阻尼器動力特性的數學模型，而且對其參數進行了辨識，通過實驗証明，該模型精確地預測了實際阻尼器的物理特性。 本論文研究了安裝有磁流變阻尼器的單自由度懸掛系統的運動特性。 同時，考慮載荷具有不確定性，因此建立了一個滑模控制器以實現懸掛系統的魯棒控制。 爲了研究懸掛系統的性能，本論文採用了兩種不同的激勵，而且對響應在時間和頻率領域同時進行了分析。 與被動控制系統相比，通過安裝受控的磁流變阻尼器，簧載質量的加速度和位移均大幅度被減低。 在隨機激勵的情況下，磁流變阻尼器也同時表現了對峰值響應和方根平均值響應的減振能力。

ABSTRACT

Semi-active control systems are becoming more popular because they offer both the reliability of passive systems and the versatility of active control systems without imposing heavy power demands. It has been found that magnetorheological (MR) fluids can be designed to be very effective vibration control actuators. MR fluid damper is a semi-active control device that uses MR fluids to produce controllable damping force. The objective of this thesis is to study a single-degree-of-freedom (SDOF) suspension system with a MR fluid damper for the purpose of vibration control. A mathematical model of MR fluid damper is adopted. The model is compared with experimental results for a prototype damper through finding suitable model parameters. The motion characteristics of the SDOF suspension system with MR damper are studied and compared with those of system with conventional viscous damper. In this thesis, a sliding mode controller is developed by considering loading uncertainty to result in a robust control system. Two kinds of excitations are inputted in order to investigate the performance of the suspension system. The vibration responses are evaluated in both time and frequency domains. Compared to the passive system, the acceleration and displacement of the sprung mass are significantly reduced for the system with a controlled MR damper. Under random excitation, the ability of the MR fluid damper to reduce both peak response and root-mean-square response is also shown.

ACKNOWLEDGEMENTS

I would like to sincerely thank my thesis advisor, Prof. Liao Wei-Hsin, for his guidance, support and encouragement over the past two years. More importantly, he taught me that one needed both aggressive attitude and patience to become a successful researcher.

I would also like to thank Prof. Li Wen-Jung and Prof. Yam Yeung who were my committee members, as well as other faculty members for their patient instruction throughout my academic study at The Chinese University of Hong Kong.

Also, I would like to express my thanks to Mr. Allan Mok, Mr. Tong Hang and Mr. Martin Leung for their technical advices on my project, and my close colleagues, Mr. Alan Lam and Mr. Wilson Yu, for the research support to my work. Their insights and advices enabled me to break through problems and certainly resulted in timely completion of this thesis. Also, I wish to express extra thanks to Dr. Wang Dai-Hua for translating the abstract to the Chinese version.

Finally, from the bottom of my heart, I thank CY for being there with me in many long lonely nights.

TABLE OF CONTENTS

LIST OF FIGURES ..... **vi**

LIST OF TABLES ..... **ix**

1 INTRODUCTION **1**

1.1 Background 1

1.1.1 Vibration Control of Suspension Systems 1

1.1.2 Semi-active Devices 3

1.2 Literature Review 5

1.2.1 MR Fluid and Damper 5

1.2.2 Vibration Control 6

1.2.3 Robust Control 8

1.3 Research Objective 9

1.4 Organization of the Thesis 9

2 MR DAMPER BEHAVIOR AND MODELING **11**

2.1 MR Damper 12

2.2 Mathematical Model 13

2.3 Experimental Setup 15

2.4 Damper Characteristics 18

2.5 Comparison Between Model with Experimental Data 25

2.5.1 Graphical Study 26

2.5.2 Quantitative Study 26

2.5.3 Other Input Tests 27

3 SEMI-ACTIVE VIBRATION CONTROL 33

3.1 Dynamic Modelling of Suspension Systems 33

3.2 Single-degree-of-freedom (SDOF) Passive Suspension System 34

3.2.1 Viscous Damper 34

3.2.2 MR Damper 37

3.3 Single-degree-of-freedom (SDOF) Semi-active Suspension System 41

3.3.1 Ideal Skyhook Control 41

3.3.2 Semi-active Skyhook Control 44

3.4 Semi-active Robust Control Development 46

3.5 Sliding Mode Control 47

3.6 Semi-active Damper Control 51

3.6.1 On-off Control 52

3.6.2 Continuous-state Control 53

3.6.3 Comparison Between On-off and Continuous-state Controller 54

4 SIMULATION STUDIES 57

4.1 Transmissibility 57

4.2 Different Base Excitations 59

4.2.1 Bump Input 60

4.2.2 Random Input 62

5 CONCLUSION 67

5.1 Summary 67

5.2 Future Work 68

APPENDIX 69

A.1 Semi-active Control with MR Damper – Main Program Listing 69

A.2 Sub-program Listing (Dynamic System) 70

A.3 Sub-program Listing (Sliding Mode Controller) 73

A.4 Sub-program Listing (MR Damper Model) 73

BIBLIOGRAPHY 75

LIST OF FIGURES

Figure 2.1: Linear damper characteristics 11

Figure 2.2: Ideal MR damper performance 12

Figure 2.3: MR damper 12

Figure 2.4: Schematic of the MR damper 12

Figure 2.5: Mechanical model of the MR damper 14

Figure 2.6: Schematic test setup for MR damper 16

Figure 2.7: Experimental setup 16

Figure 2.8: Highlighted experiment setup 16

Figure 2.9: Controller for the shaker 16

Figure 2.10: Overview of the data acquisition 17

Figure 2.11: Damping force under sinusoidal excitation at 1 volt 18

Figure 2.12: Force-displacement relation of MR damper 19

Figure 2.13: Force-velocity relation of MR damper 19

Figure 2.14: Force vs. voltage at different velocities 19

Figure 2.15: Force-displacement relation with different excitation amplitude 21

Figure 2.16: Energy dissipated vs. voltage 21

Figure 2.17: Energy dissipated vs. displacement amplitude 21

Figure 2.18: Energy dissipated vs. frequency 21

Figure 2.19: Equivalent damping coefficient vs. input voltage 23

Figure 2.20: Equivalent damping coefficient vs. displacement amplitude 23

Figure 2.21: Equivalent damping coefficient vs. frequency 23

Figure 2.22: Comparison of model and experimental results 26

Figure 2.23: Current driver 27

Figure 2.24: Current driver circuit for MR damper 28

Figure 2.25: First test for the model of the damper 29

Figure 2.26: Second test for the model of the damper 29

Figure 2.27: Third test for the model of the damper 30

Figure 2.28: Final test for the model of the damper 31

Figure 3.1: Single-degree-of-freedom system 33

Figure 3.2: Single-degree-of-freedom system with MR damper 33

Figure 3.3: Transmissibility and phase for the passive suspension with viscous damper 37

Figure 3.4: Transmissibility and phase for the passive suspension with MR damper 38

Figure 3.5: Relative displacement of the SDOF system 39

Figure 3.6: Equivalent damping coefficient for each voltage 39

Figure 3.7: Comparison between two transmissibilities of SDOF system 40

Figure 3.8: SDOF system with skyhook configuration 41

Figure 3.9: Transmissibility and phase for the ideal semi-active suspension 43

Figure 3.10: Semi-active suspension system 44

Figure 3.11: Block diagram of the semi-active control system 46

Figure 3.12: Sliding condition 48

Figure 3.13: Structure of the sliding mode active suspension system 51

Figure 3.14: Graphical representation of the on-off control 53

Figure 3.15: Structure of the continuous-state control 54

Figure 3.16: First test for the damper controller 55

Figure 3.17: Second test for the damper controller 55

Figure 3.18: Corresponding velocity of MR damper in second test 56

Figure 4.1: Transmissibility of the controlled system with maximum input 1 volt.....58

Figure 4.2: Transmissibility of the controlled system with maximum input 2 volts 58

Figure 4.3: Two displacement excitations to the system for simulations 59

Figure 4.4: System responses under bump input using active control (with perturbation) 60

Figure 4.5: System responses under bump input (without perturbation).....61

Figure 4.6: System responses under bump input (with perturbation) 62

Figure 4.7: Frequency responses under random input using active control (with perturbation).....63

Figure 4.8: Frequency responses under random input (without perturbation).....64

Figure 4.9: Frequency responses under random input (with perturbation).....65

LIST OF TABLES

Table 1.1: Summary of the properties of ER and MR fluids [5] 4

Table 2.1: Parameters for the model 25

Table 2.2: Model errors 27

Table 3.1: Tracking error of the damping force 55

Table 4.1: Comparison under random excitation 65

CHAPTER ONE

INTRODUCTION

1.1 Background

1.1.1 Vibration Control of Suspension Systems

Suspension systems can be used to control vibration of various rigid and flexible modes of vehicles. They reduce the motion and acceleration of the sprung mass in a vehicle. Vibration in today's increasingly high-speed vehicles severely affects their ride comfort. In the environment of a moving vehicle, ride quality is concerned with the sensation or feel of the passenger. To improve the ride comfort, effective vibration control of vehicle suspension systems is increasingly necessary. A suspension system must support the weight of the vehicle and provide effective isolation of passengers and payload from road disturbances. A passive suspension system has the ability to store energy via a spring and to dissipate it via a damper. The parameters are generally fixed, being chosen to achieve a certain satisfactory performance. Once the spring has been selected based on the load-carrying capability of the suspension, the damper is the only variable remaining to be specified. Low damping yields poor resonance control at the natural frequencies of the system but provides the high frequency isolation. Conversely, large damping results in good resonance control at the expense of high frequency isolation. So, the passive system has its own limitation due to these conflicting demands. In order to deal with the problem, active control has been proposed for vibration control.

In a passive system, the parameters are synthesized through off-line design techniques and no on-line feedback actions are used. Since passive systems produce fixed designs, the control will not be optimal when the system or the operating condition changes. On the other hand, active controls have been of popular interest in recent years. Force or torque inputs from actuators are usually used to suppress vibration amplitudes based on on-line measurements from sensors. The advantage of an active approach is that it can adapt for system variations, and thus, can be much more effective than passive systems. It has advantages over passive systems for desirable performance. However, such a system requires large amounts of power and is thus somehow impractical for some applications. In addition, if such a system should fail, it would be left with no significant damping, which can yield an unstable condition.

Because of the difficulties encountered in using a purely active suspension, it is often more beneficial to use a semi-active suspension. During the past decade, semi-active vibration control has been investigated by several researchers [1-3]. The devices used in a semi-active system are ones which will not input energy to the system but adaptable. This kind of system combines the features of active and passive systems. Certain control actions are regulated by algorithms using measured excitation and response in the semi-active system. Such systems potentially offer the reliability of the passive system. Even if the power to the semi-active system is lost, the system can still provide a certain level of damping, making it safer than a purely active one. On the other hand, they maintain the adaptability as the active systems have. At the same time, unlike in the case of active system, since no energy is inputted directly to the system, the

energy required for certain control action is much less. So, compared with active control, a semi-active one requires less power consumption and less complicated hardware.

1.1.2 Semi-active Devices

There are two methods for creating a damper with variable damping: changing the size of the orifice through which the hydraulic fluid passes, and changing the properties of the fluid itself. The orifice size can be changed by using a motor or some other actuators to open and close it. To implement a damper where the properties of the fluid change, there are two types of materials available: magnetorheological (MR) and electrorheological (ER) fluids.

As the name implies, ER fluids are a class of fluids in which the rheological properties of the fluid are changed by subjecting the fluid to an electric field. MR fluids are magnetic analogs of ER fluids and typically consist of micron-sized, magnetically polarizable particles dispersed in a carrier medium such as mineral or silicone oil. When a magnetic field is applied to the fluid, particle chains form, and the fluid becomes a semi-solid and exhibits viscoplastic behavior similar to that of ER fluid. However, the yield stress of MR fluids is significantly greater than that of their ER counterparts. When applying a magnetic field, the yield stress values more than 80 kPa are easily obtained. With such high yield stress, the power required is much smaller than that for ER fluid. It can operate at temperatures from – 40 to 150 °C [4]. The yield strength varies only slightly over this range. A change in the particles' volume fraction due to expansion and contraction of the carrier fluid over the temperature change produces the variation. MR fluids can respond to an applied magnetic field within milliseconds. The

compliance of a particular device and the rate at which the magnetic field is generated are two key factors affecting the response time. Unlike ER fluids, MR fluids are not affected by chemical impurities normally produced during manufacturing and use. Also, its raw materials are nontoxic and environmentally safe [4]. The controllable change of state with some desirable features such as high strength, good stability, broad operational temperature range, and fast response time give rise to vehicle suspension system applications. The summary of the properties of typical ER and MR fluids are shown in Table 1.1.

Table 1.1: Summary of the properties of ER and MR fluids [5]

Property	ER fluid	MR fluid
Yield Strength	2-5 kPa (3-5 kV/mm) Field Limited by Breakdown	50-100 kPa (150-250 kA/m) Field Limited by Saturation
Viscosity (No Field)	0.2-0.3 Pa-s @ 25 °C	0.2-0.3 Pa-s @ 25 °C
Operating Temperature	+10 to +90 °C (ionic, DC) -25 to +125 °C (non-ionic, AC)	-40 to +150 °C (limited by carrier fluid)
Specific Gravity	1-2.5	3-4
Ancillary Materials	Any (conductive surfaces)	Iron/Steel
Color	Any, Opaque or Transparent	Brown, Black, Gray/Opaque

MR fluid dampers considered in this thesis are semi-active control devices that use MR fluids to produce controllable damping forces. The MR fluid essentially allows one to control the damping force of the damper by replacing mechanical valves commonly used in adjustable dampers. This offers the potential for a superior damper with little concern about reliability since if the MR damper ceases to be controllable, it

simply reverts to a passive damper. While purely active force generators are capable of providing an arbitrary force to the system, the MR dampers produce damping force in a semi-active manner.

1.2 Literature Review

1.2.1 MR Fluid and Damper

It has been found that MR fluids can be quite promising for vibration reduction applications [6]. The following are those researches about characterizing the properties of MR fluids. Lazareva and Shitik [7] studied the properties of MR fluids that were based on barium, strontium ferrites and iron oxides. The fluids were prepared using various combinations of the materials, and their properties, such as the MR effects, were studied. Ashour et al. [8] studied the effects of components of the MR fluid on sedimentation of the magnetic particles and initial viscosity. An attempt was made to optimize the composition of the fluid such that the fluid had the desired properties. In another study, Ashour et al. [9] studied the general composition of MR fluid along with the methods that were used to evaluate the performance of the fluids. There was also an introduction to the fundamental MR devices that exploit the MR effect.

The following studies explored the design of MR fluid devices. Carlson et al. [5] studied the advantages of MR over ER fluid devices in areas such as the yield strength, the required working volume of fluid, and the required power. The operational modes of the MR fluid were presented along with the linear fluid damper, the rotary brake, and the vibration damper. Kordonsky [10] developed the concept of the MR converter (or valve)

and applied the MR converter to create devices such as the MR linear damper, the MR actuator, and the MR seal. Finally, Bolter and Janocha [11] examined the rules that should be applied when designing the magnetic circuit for MR devices that are working in the different modes of the MR fluid. They also examined the use of permanent magnets in the design of the magnetic circuit to change the operational point of the MR device.

Viscoelastic-plastic model was considered by Li et al. [12] to model a MR damper. Also, The hysteresis behavior of the linear stroke magnetorheological damper was characterized by four different nonlinear models [13]. It was proved that all of them could be used successfully if only a good prediction of energy dissipation or damping was of concern. An alternative representation of MR damper in terms of neural network was developed by Chang and Roschke [14]. It was shown that the model together with the system identification theory is a good alternative for special characterization of an MR damper.

1.2.2 Vibration Control

Many researches in the area of semi-active suspensions have been conducted. Lieh [15] explored the use of semi-active suspensions to control the dynamics of a full car model. He concluded that the skyhook control policy reduces the root-mean-square (RMS) acceleration of the car body while increasing the RMS tire forces. Also, Taghirad and Esmailzadeh [16] have studied the effect of optimal active suspension on ride performance. The study by Margolis [17] examined the effects of using realistic feedback signals when controlling active and semi-active suspension systems. This was

an analytical study that suggested several feedback strategies for the semi-active suspension system so that the performance can approach the fully active suspension performance.

Hwang et al. [18] presented an interesting method for testing the semi-active damper hardware without using a complete vehicle. They explored the test method known as a Hardware-In-the-Loop (HIL) simulation. Essentially, the dynamic model of the system was coded for simulation in a computer. The piece of hardware under test (i.e. the semi-active damper) was excited according to the computer numerical simulation, and the response of the hardware was measured and fed back into the computer to complete the simulation. Miller [19] explored the effects of the levels of both on-state and off-state damping on the performance of the quarter-car semi-active suspension systems. Wu and Griffin [20] developed a semi-active on-off control policy for reducing end-stop impacts in suspension seat with an ER damper. A seat suspension system, equipped with skyhook control scheme, using a MR damper has been developed by Choi et al. [21].

Karnopp [22] contributed an excellent review of many of the past efforts in the area of semi-active suspension design. He also presented a background of the information that was required to understand semi-active suspension systems. Finally, he discussed several semi-active suspension applications. Cebon et al. [23] discussed the different control strategies that were available for two-degree-of-freedom semi-active systems. They applied semi-active control and linear optimal control with full-state feedback along with simple on-off control strategies in order to reduce both the tire force and body acceleration of a heavy truck. They compared the results of their mathematical

simulations to their experimental results using a HIL test method. They concluded that, compared to passive suspensions, the full state feedback methods work the best in reducing tire loads and body acceleration according to simulation and experimental results. Finally, the skyhook study by Satoh et al. [24] was a practical realization of a fully active skyhook suspension system on a passenger vehicle. The controller responded to a pitch and roll motions of the vehicle, as well as to the vertical motion of the wheels. The results in an actual vehicle showed marked improvement over the passive suspension.

1.2.3 Robust Control

Since system dynamics changes with parameters, a sliding mode controller has been designed and applied on a half-car suspension system [25]. The results of this study proved that the performance of active suspension using this control is better than that of passive system. A method based on sliding mode control for the design of a quarter-car model following active suspension has been presented by Mohan [26]. It ensured that the system can follow the reference system even if the suspension parameters change rapidly in a given range. Titli et al. [27] compared the designs of semi-active suspension with optimal controller, sliding mode controller and fuzzy controller on quarter-car model. Their performances were tested by simulation on more realistic models including non-linearities and time delays. A sliding mode control strategy was proposed to suppress structural vibration using ER fluid [28]. Analysis on a beam example was carried out to examine the effectiveness of the control law. The

example showed that it was feasible to vary (online) the structural stiffness and damping by using a distributed ER fluid material in the structure.

Hung et al. [29] introduced the fundamental theory, main results and practical applications of the variable structure control system design approach. Also, some future research areas were suggested. Decarlo et al. [30] presented the design of variable structure control systems for a class of multivariable nonlinear time varying systems in a tutorial manner. Besides, the paper investigated the applications and developments of this powerful control.

1.3 Research Objective

The aim of this study is to investigate the fundamental characteristics of the MR damper and the suspension system with the damper in order to develop a vibration control method for the system. Even in the presence of loading uncertainty within the system, employing a robust controller, the vibration suppression can still be successful. Specifically, the simulation results of sliding mode control will be used to evaluate the performance of such suspension system, compared with the passive systems.

1.4 Organization of the Thesis

This dissertation is divided into 5 chapters. Chapter 1 gives an introduction of the study and presents the literature survey such as accomplishments and achievements of previous related researches. Chapter 2 describes the operational principle and the

mathematical model of the MR damper. Also, the characteristics of the damper will be illustrated through several sets of experiments in this chapter. Chapter 3 shows, in detail, the overall picture of the controlled system. Before that, the characteristics of the single-degree-of-freedom (SDOF) system with a MR damper will be studied. The simulation results of the system compared with the passive systems will be analyzed in Chapter 4. Finally, in Chapter 5, the results of this study will be summarized and recommendations for future work regarding this project will be presented.

CHAPTER TWO

MR DAMPER BEHAVIOR AND MODELING

For a typical passive damper, the damper performance is often evaluated based on the force vs. velocity characteristics. For a linear viscous damper, the force vs. velocity relation is shown in Figure 2.1. The slope of the force vs. velocity line is known as the damping coefficient.

Since the characteristics of a passive damper are such that there is only one force corresponding to given velocity, the damping curve is tuned by a ride engineer for each particular application. Therefore, the operational envelope of a passive damper is confined to one pre-designed force-velocity characteristic.

In the case of MR dampers, the ideal force-velocity characteristics are shown in Figure 2.2. The result is a force vs. velocity envelope that is spanned by an area rather than a line in the force-velocity of a linear damper. Effectively, the controller can be programmed to emulate any damper force-velocity characteristic within envelope.

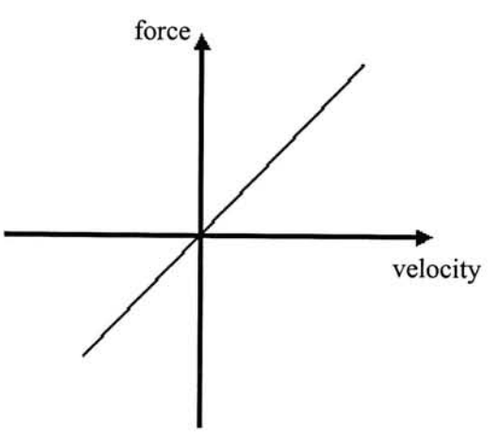


Figure 2.1: Linear damper characteristics

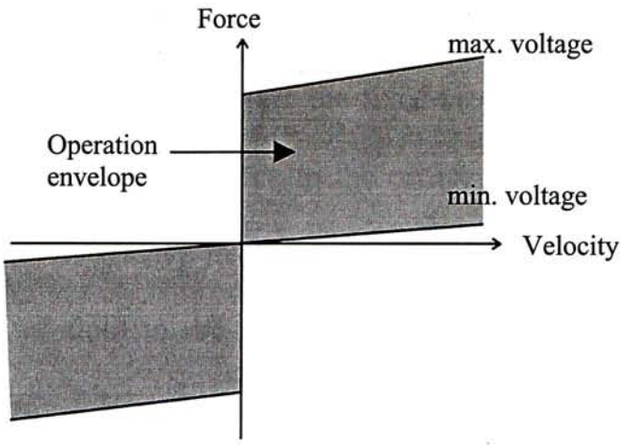


Figure 2.2: Ideal MR damper performance

2.1 MR Damper

Figure 2.3 shows the MR damper (RD-1005-1 manufactured by Lord Corporation) used in this study. The schematic diagram of this damper is shown in Figure 2.4. The length of the damper is 208.3 cm in its extended position. It has a 5 cm stroke. The maximum current to the electromagnet in the magnetic choke is 2 A and the coil resistance is 5 Ω.



Figure 2.3: MR damper

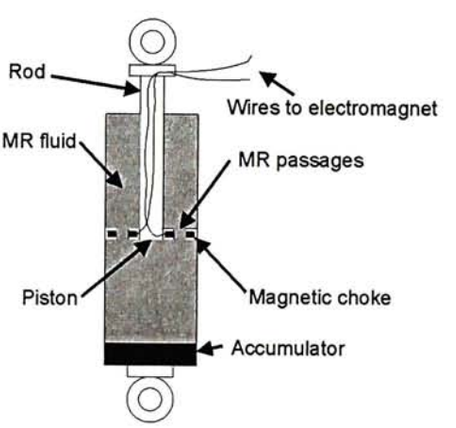


Figure 2.4: Schematic of the MR damper

The fluid that is transferred from above the piston to below (and vice versa) must pass through two valves. The MR valves are the fixed-size orifices with the ability to apply a magnetic field, using electromagnet, to the orifice volume. For each volume, this magnetic field results in a change in viscosity of the MR fluid, causing a pressure differential for the flow of fluid in the orifice volume. The pressure differential is directly proportional to the force required to move the damper rod. As such, the damping characteristic of the MR damper is a function of the electrical current flowing into the electromagnet. This relationship allows the damping of an MR damper to be easily controlled in real time.

The accumulator is a pressurized volume of gas that is physically separated from the MR fluid by a bladder. The accumulator has two purposes. The first is to provide a volume for the MR fluid to occupy when the shaft is inserted into the damper cylinder. The second is to provide a pressure offset so that the pressure in the low pressure side of the MR valve does not induce cavitation in the MR fluid by reducing the pressure below the vapor pressure of the MR fluid.

2.2 Mathematical Model

To evaluate the potential of MR dampers in vibration control application and to take full advantage of the unique features of these devices, a model must be developed that can accurately represent the behavior of the MR damper. Experiments are set up to obtain data for identification of a model for the MR damper used in this study. Based on

the experimental data, a least-square optimization method is employed to determine appropriate parameters for the analytical model.

The mathematical model proposed by Spencer et al. [31] is adopted in this study. The hysteretic behavior in the damper is described by the Bouc-Wen model [32].

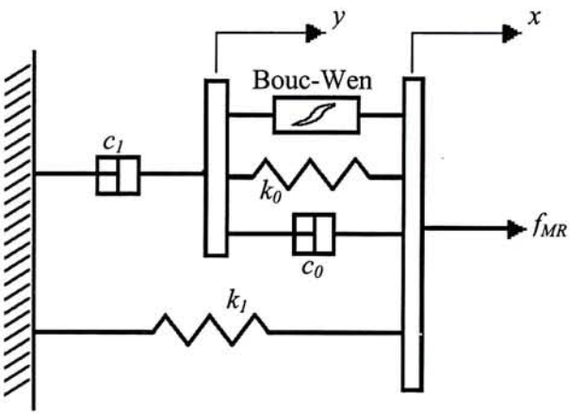


Figure 2.5: Mechanical model of the MR damper

Under constant magnetic fields, the system in Figure 2.5 will be considered. To obtain the governing equations for this model, consider only the upper part of the model. The resultant force on the rigid bar is zero.

$$\dot{y} = \frac{1}{(c_0 + c_1)}\left[\alpha z + k_0(x - y) + c_0\dot{x}\right] \tag{2.1}$$

where z is given by

$$\dot{z} = -\gamma|\dot{x} - \dot{y}||z|^{n-1} z - \mu(\dot{x} - \dot{y})|z|^n + A(\dot{x} - \dot{y}) \tag{2.2}$$

The total force generated by the system is then found by summing the forces in the upper and lower sections of the system in Figure 2.5, yielding

$$f_{MR} = c_1\dot{y} + k_1(x - x_0) \tag{2.3}$$

x_0 is used to account for the effect of the accumulator. α is a scaling value for the Bouc-Wen model. The scale and shape of the hysteresis loop can be controlled by γ, μ, A and n. Until now, only the case for the constant electrical input is considered. In

order to adapt to the environment, a model which can represent changing voltage input should be used. To determine a model that is valid for fluctuating magnetic fields, the dependence of the parameters on the applied current must be determined. Therefore, the following linear relations have been proposed [31]:

$$\alpha = \alpha(u) = \alpha_a + \alpha_b u \tag{2.4}$$

$$c_1 = c_1(u) = c_{1a} + c_{1b} u \tag{2.5}$$

$$c_0 = c_0(u) = c_{0a} + c_{0b} u \tag{2.6}$$

u is given by the following dynamic equation:

$$\dot{u} = -\eta(u - v) \tag{2.7}$$

where v is the voltage applied to the current driver. Eq. (2.7) models the reaching rheological equilibrium of the MR fluid due to the change of magnetic field. The rate of reaching equilibrium is governed by η.

The optimized values for the 14 parameters (c_{0a}, c_{0b}, k_0, c_{1a}, c_{1b}, k_1, x_0, α_a, α_b, γ, μ, A, n, η) are determined to fit the model to the experimental data obtained in the experiments.

2.3 Experimental Setup

The load frame shown in Figure 2.6 is set up and built for the purpose of obtaining MR damper response data for parameter identification. The actual experimental setup is shown in Figure 2.7. The dynamic responses of the damper can be measured for a wide range of prescribed waveforms and frequencies.

The highlighted picture of the experiment setup is shown in Figure 2.8. The vibration system (Labworks Inc., LW-127-500) is used to produce excitation for the damper. It consists of a shaker (ET-127) and a matching linear direct coupled power amplifier (PA-123-3/2-500). The amplifier (see Figure 2.9) receives electrical signal, amplifies and sends it to the shaker. The load cell (PCB Piezotronics Inc., 208C03) can sense the damping force under different conditions. A laser vibrometer (Polytec GMBH, OFV-3001) is used to measure the related displacement and velocity.

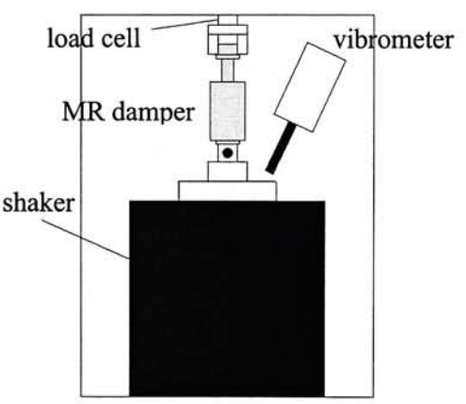


Figure 2.6: Schematic test setup for MR damper



Figure 2.7: Experimental setup

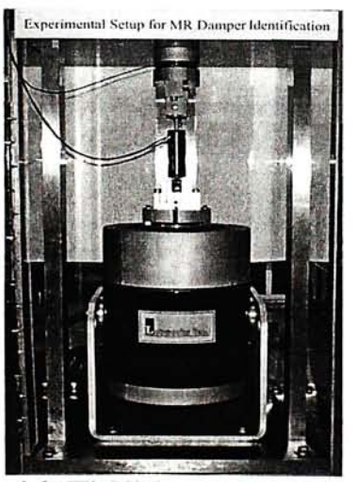


Figure 2.8: Highlighted experiment setup

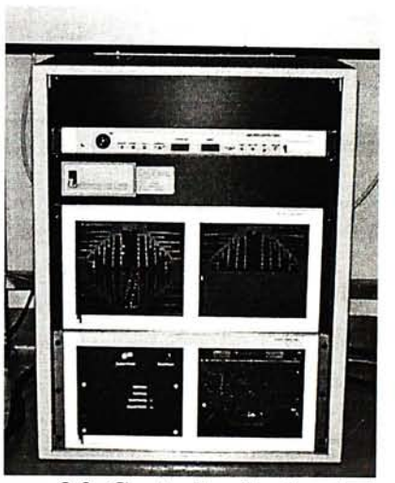


Figure 2.9: Controller for the shaker

In order to acquire the experimental data (displacement, velocity and damping force of the MR damper), the dSPACE system is used. It also commands the suitable

voltage signal to the MR damper. In general, the dSPACE system is a powerful tool designed for rapid prototyping of controllers. It consists of two main elements – software and hardware. The software interfaces with MATLAB on a PC and allows the user to create a block diagram of the system in Simulink. The dSPACE Real-Time Interface, which runs under MATLAB, can then compile the Simulink model and load the model directly to a DSP chip in the hardware element of the dSPACE system. The hardware portion consists of the DSP processor board. The dSPACE system reduces the job of designing and prototyping controllers to simply building a model in Simulink and downloading the program to the DSP board with the press of a button. All data for this research were acquired directly using the TRACE module in the dSPACE toolkit. TRACE can generate a time history of any variable in the Simulink control block diagram. Figure 2.10 shows the overall picture of the data acquisition for the damper testing.

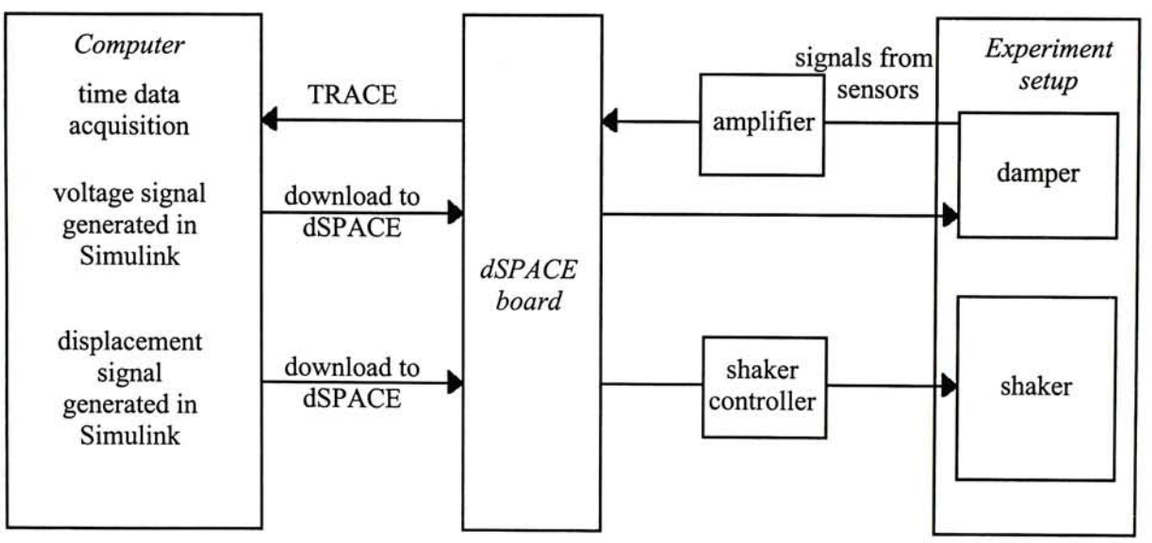


Figure 2.10: Overview of the data acquisition

2.4 *Damper Characteristics*

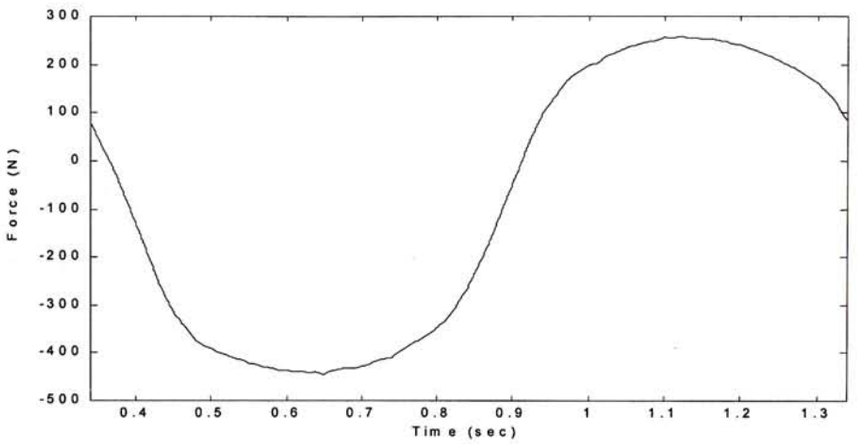


Figure 2.11: Damping force under sinusoidal excitation at 1 volt

In this experiment, the shaker is driven with a sinusoidal signal with a fixed frequency, and the voltage applied to the damper is held at a constant level. Three sets of experimental data are obtained according to three voltage levels (0V, 1V, and 2V). Each set of data consists of displacement, velocity and damping force. All of them are recorded as a function of time. For example, when the input voltage is 1 volt, the damping force with 1 Hz excitation is recorded and shown in Figure 2.11.

The responses of the MR damper due to a 1 Hz sinusoidal signal are shown in Figures 2.12 and 2.13 for three constant voltage levels applied to the damper. Both force-displacement and force-velocity loops are shown in these two figures. The force-displacement loops (Figure 2.12) progress along a clockwise path with the increase of time while the force-velocity loops (Figure 2.13) progress along an anti-clockwise path. Also, it can be seen that, as the voltage increases, the corresponding damping force increases.

For Figure 2.12, the force produced by the damper is not centered at zero. This shows the effect of the accumulator in the bottom of the damper. From both Figures

2.12 and 2.13, the maximum force increases with increasing applied voltage which is related with the magnetic field.

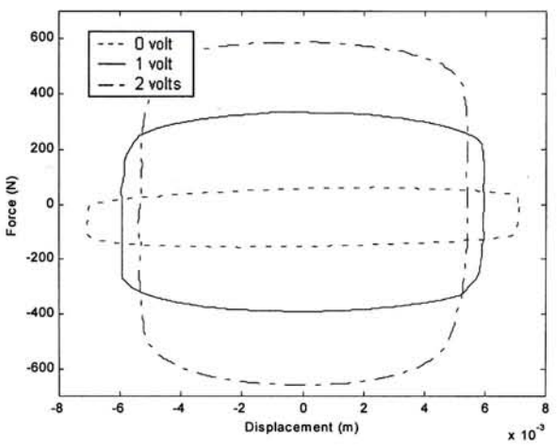


Figure 2.12: Force-displacement relation of MR damper

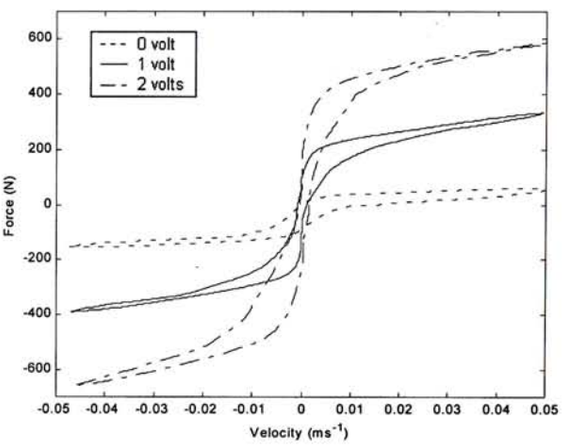


Figure 2.13: Force-velocity relation of MR damper

Also, the force for a given velocity is approximately linear to the applied voltage. This characteristics can be seen obviously in Figure 2.14. The value next to each mark is the voltage applied. The values of the damping forces are picked from Figure 2.13. For positive velocity, the values are from the upper part of the curve. For negative velocity, they are from the lower part of the curve.

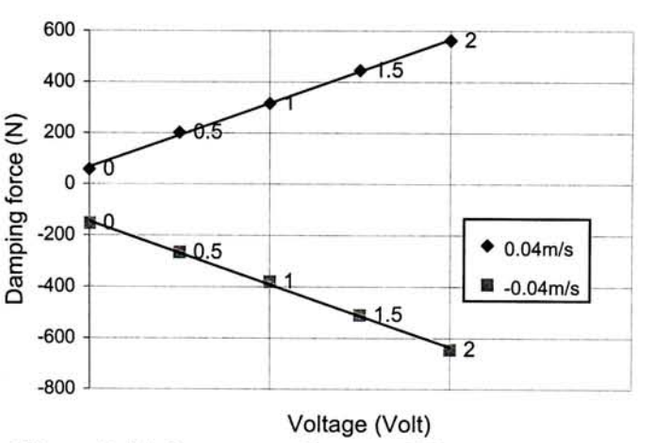


Figure 2.14: Force vs. voltage at different velocities

As shown in Figure 2.13, when the damper restoring force is less than the yield force, the damper is operating in the pre-yield region. It strongly exhibits the hysteresis characteristics. Also, the slope of the curve is relatively steep. When the restoring force

is larger than the yield force, it is operating in the post-yield region. The yield transition occurs as the damper restoring force crosses the yield force value. After the yield force values, the rate of change of damping force with velocity is relatively low.

In order to compare the damping performance of the MR damper with that of a conventional viscous damper, an equivalent damping coefficient c_{eq} is determined by equating the energy dissipated in a full cycle [12]. In the following experiments, sinusoidal excitations with different amplitudes are used to test this characteristic under different voltages inputs. For example, with no voltage input, five sets of data (peak amplitudes of excitations are 0.002 m, 0.004 m, 0.006 m, 0.008 m and 0.01 m), under 1 Hz excitation, are captured and five sets of force vs. velocity are shown in Figure 2.15.

In a similar way, some experiments are done under sinusoidal excitations with different frequencies (0.2 Hz, 0.6 Hz, 1 Hz, 1.4 Hz and 1.8 Hz) with fixed excitation amplitude.

Let the energy dissipated by the MR damper in one cycle be W

$$W = \int_0^{\frac{2\pi}{\omega_d}} F_{MR} dx \tag{2.8}$$

Substitute $F_{MR} = c_{eq}\dot{x}$,

$$W = \int_0^{\frac{2\pi}{\omega_d}} c_{eq}\dot{x} dx \tag{2.9}$$

where ω_d is the driving frequency of the sinusoidal excitation

$\dot{x}$ is the relative velocity of the damper

F_{MR} is the measured damping force

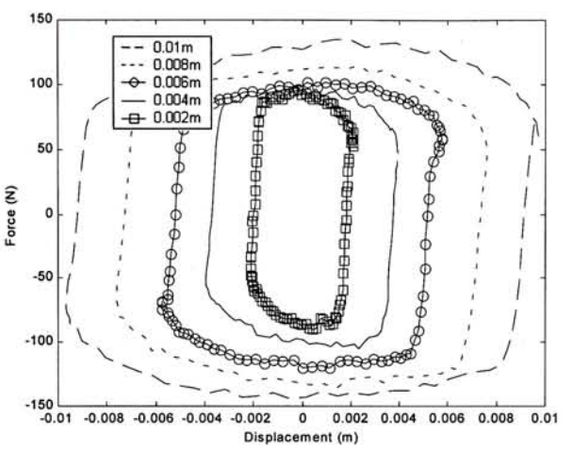


Figure 2.15: Force-displacement relation with different excitation amplitude

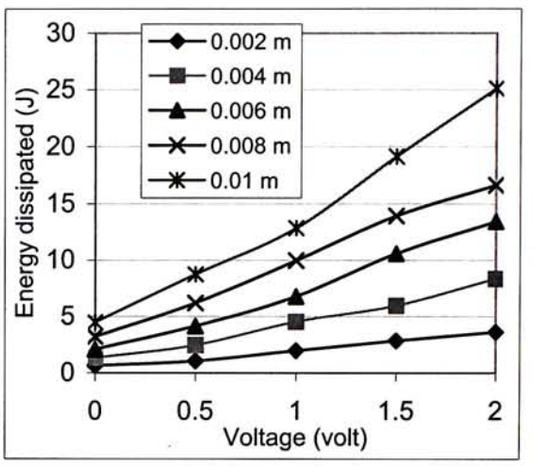


Figure 2.16: Energy dissipated vs. voltage

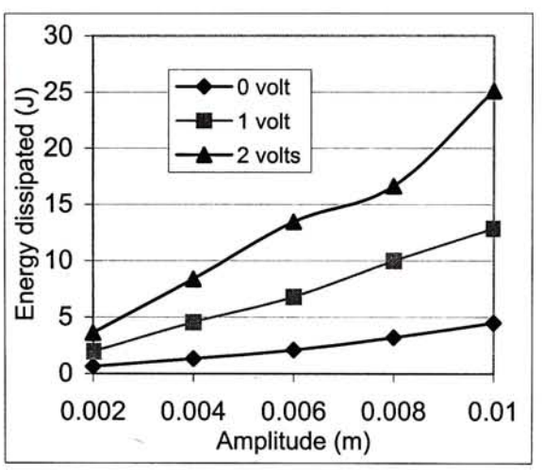


Figure 2.17: Energy dissipated vs. displacement amplitude

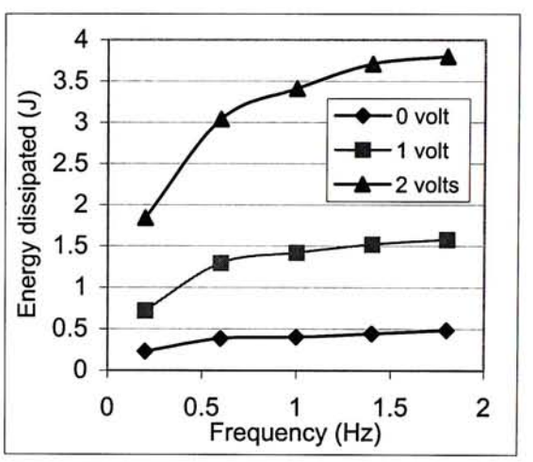


Figure 2.18: Energy dissipated vs. frequency

It should be noted that W can be found out by the area enclosed by the curve in Figure 2.15 under particular voltage input, excitation amplitude, and frequency. Then, the energy dissipated per cycle in each case can be calculated. The relations among W, input voltage, excitation amplitude and frequency are shown in Figures 2.16 - 2.18. The excitation frequency for the results shown in Figures 2.16 and 2.17 is 1 Hz. For Figure 2.18, while the excitation amplitude is kept constant (0.004 m peak-peak), the excitation frequency and voltage input are to be varied. From Figure 2.15, it is obvious that a greater energy dissipated is resulted from a greater excitation amplitude due to a larger loop. Also, for higher voltage input, the loop will be larger due to the higher damping

force. This results in a larger amount of energy dissipated. These results are also shown in Figures 2.16 and 2.17.

Observing Figure 2.18, for the same voltage input, the variance of the energy dissipated under excitation of higher frequency is less than that under one of low frequency. This shows that, at higher frequency, the energy dissipated varies little with the excitation frequency for a fixed amplitude. As mentioned before, the energy can be found out by the area enclosed by the force-displacement loop, such as those in Figure 2.15. For MR damper, the force-displacement loop is in a rectangular shape. So, the area of the loop can be estimated by the product of peak-peak value of the displacement and that of the damping force. If the excitation amplitude is fixed, since it has been mentioned that the energy dissipated varies little with the excitation frequency at higher frequency, the peak-peak value of damping force also varies little. That means, at higher frequency, the excitation frequency does not affect the damping force too much for a fixed amplitude.

From Eq. (2.9), assuming a simple harmonic excitation as $x(t) = Y \sin \omega_d t$, where Y is the amplitude of the relative motion of the damper,

$$\begin{aligned} W &= \int_0^{\frac{2\pi}{\omega_d}} c_{eq} (\dot{x})^2 \, dt \\ &= \int_0^{\frac{2\pi}{\omega_d}} c_{eq} (\omega_d Y \cos \omega_d t)^2 \, dt \end{aligned}$$

So,

$$W = \pi c_{eq} \omega_d Y^2 \tag{2.10}$$

So, c_{eq} can be found as

$$c_{eq} = \frac{W}{\pi \omega_d Y^2} \tag{2.11}$$

The relations among c_{eq}, input voltage, excitation amplitude and frequency are shown in Figures 2.19 – 2.21. The damping coefficients in Figures 2.19, 2.20 and 2.21 correspond to the energy dissipated shown in Figures 2.16, 2.17 and 2.18 respectively.

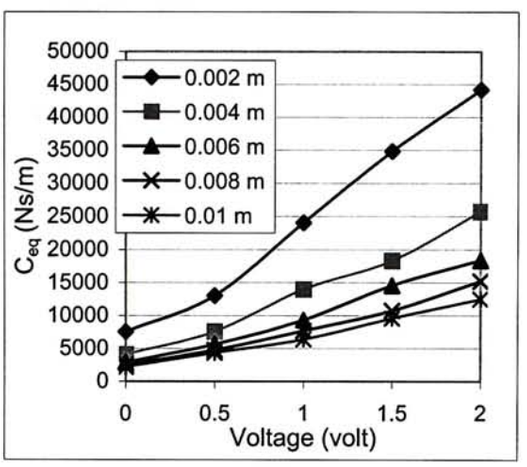


Figure 2.19: Equivalent damping coefficient vs. input voltage

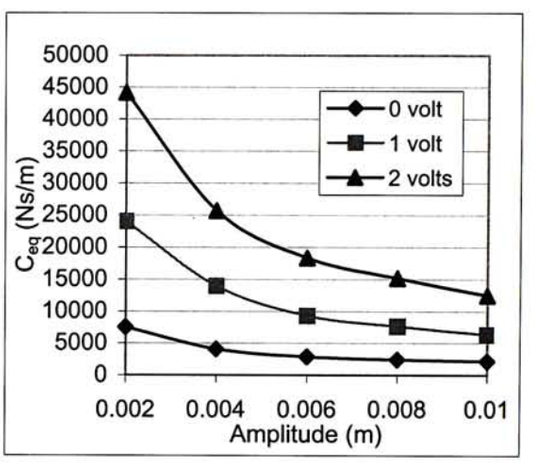


Figure 2.20: Equivalent damping coefficient vs. displacement amplitude

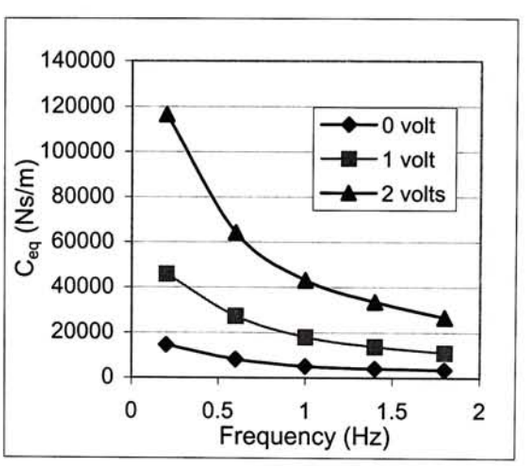


Figure 2.21: Equivalent damping coefficient vs. frequency

Figure 2.19 shows that the damping coefficient increases with the increase of the input voltage for a constant amplitude input. Also, for the amount of increase in value of c_{eq}, the effect of the increase in voltage on low amplitudes is more significant than that on high amplitudes. It presents that the value of coefficient changes dramatically with applied voltage at low amplitude where the velocity is relatively low for a fixed

frequency. For higher velocity amplitude, when the displacement amplitude is higher, the change in c_{eq} with the voltage is less in amount.

In Figure 2.20, it can be seen that the damping coefficient decreases as the excitation amplitude is raised under the same input voltage. For the same amount of increment in displacement amplitude, the coefficient for the higher voltage input decreases more. Compared with Figure 2.17 in which shows that energy dissipated increases with the excitation amplitude, it is interesting to see that the trend for the c_{eq} is opposite to that for the energy dissipated with the same voltage input. It is because, from Eq. (2.11), c_{eq} is treated as a normalized damping factor for the amount of dissipated energy with respect to excitation frequency and amplitude. From Eq. (2.11), for c_{eq}, W is divided by the square of the Y. So, for the approximately linear increase of W in Figure 2.17, c_{eq} decreases with the increase of Y.

In Figure 2.21, when the displacement (0.004 m peak-peak) is kept fixed, increase in frequency leads to the decrease in the value of damping coefficient. The amount of reduction is larger for higher voltage input. This can also be accounted for by the effect of pre-yield / post-yield phase. For lower excitation frequency, a smaller velocity will be resulted at the same excitation amplitude. Then, the damper operates in the pre-yield region. From Figure 2.13, when the fluid in the damper is in the pre-yield phase, the slope of the curve is relatively steep compared with that in the post-yield phase. Basically, the slope can reflect the damping ability which is described quantitatively by equivalent damping coefficient. When the velocity is increased, the damper would work beyond the pre-yield region. In post-yield region, the slope of

curve in Figure 2.13 is much smaller. Therefore, on average, the damping coefficient of the MR damper working at higher frequency is smaller.

2.5 *Comparison Between Model with Experimental Data*

In order to obtain the optimized parameters for the MR damper model from the above experimental data, a least-square optimization method is used. The optimization is performed using the function "leastsq" available in MATLAB. The 14 parameters are estimated by minimizing the error between the model-predicted force (f_{model}) and the force from experimental results ($f_{\text{experiment}}$). The error concerned is represented by the objective function J which is given by

$$J = \sum \left(f_{\text{experiment}} - f_{\text{model}} \right)^2 \tag{2.12}$$

It should be noted that the number of points for calculation is 400 and the sampling time is 0.005 s.

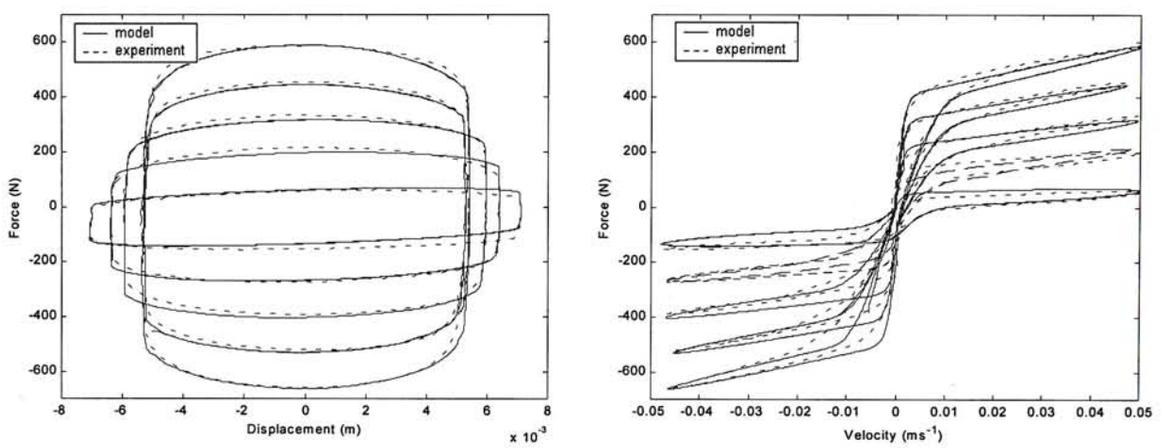
The resulting parameters are given in Table 2.1.

Table 2.1: Parameters for the model

Parameter	Value	Parameter	Value
c_{0a}	784 Ns/m	α_a	12441 N/m
c_{0b}	1803 Ns/Vm	α_b	38430 N/Vm
k_0	3610 N/m	γ	136320 /m^2
c_{1a}	14649 Ns/m	μ	2059020 /m^2
c_{1b}	34622 Ns/Vm	A	58
k_1	840 N/m	n	2
x_0	0.0245 m	η	190 /s

2.5.1 *Graphical Study*

Figure 2.22 shows the predicted model to the experimental data for five constant voltages (0 V, 0.5 V, 1 V, 1.5 V, and 2 V). It can be seen that the model accurately predicts the behaviour of the damper.



(a) Force-displacement relationship (b) Force-velocity relationship

Figure 2.22: Comparison of model and experimental results

2.5.2 *Quantitative Study*

Besides the graphical comparison, a quantitative error is used to show the performance of the model. The error is represented by

$$E = \frac{e}{\sigma} \tag{2.13}$$

where $e^2 = \sum \left(f_{\text{experiment}} - f_{\text{model}} \right)^2$ and $\sigma^2 = \sum \left(f_{\text{experiment}} - \mu_{\text{model}} \right)^2$

μ_{model} is the mean value of the damping forces of the model. The resultant error of each case is shown in Table 2.2. Those values also demonstrate the high accuracy of the model.

Table 2.2: Model errors

Voltage input (volt)	0	0.5	1	1.5	2
Error	0.194	0.0989	0.0843	0.0621	0.0861

2.5.3 Other Input Tests

In the following experiments, the power input to the MR damper is not held constant anymore. So, the varying command signal is outputted from the DSP board. Since the MR effect is a function of the current flowing through the MR coil, a circuit needs to be used to drive a current through the damper that is proportional to the control voltage from the dSPACE controller. The circuit shown in Figure 2.23 is used for this purpose.

The MR damper model with the optimal parameters in Table 2.1 will be tested under different conditions. Those tests include input signals with step voltage, random voltage, sinusoidal displacement, and random displacement.

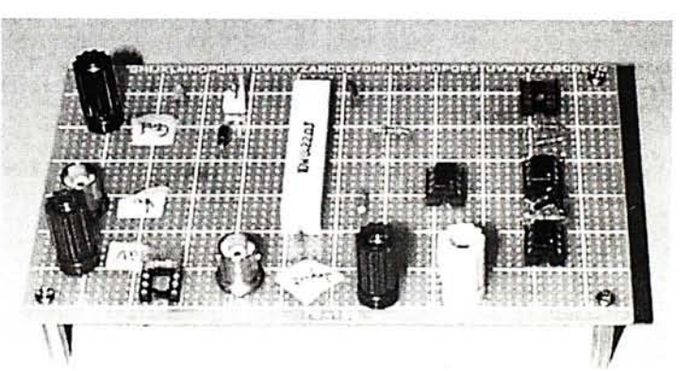


Figure 2.23: Current driver

In the following section, the test results will be described and a comparison will be made between the experimental data and the responses predicted by the model. Figure 2.24 shows the schematic diagram of the current driver circuit. The circuit takes the voltage signal from the DSP processor board and uses a power transistor to drive a

proportional amount of current through a fixed load. In the case of the MR damper, the load is actually a coil with inductance as well as resistance, and therefore is not truly fixed. However, the inductance of the coil is small and the frequency range of interest is low enough to neglect the effective resistance change of the load due to the time rate of change of the current.

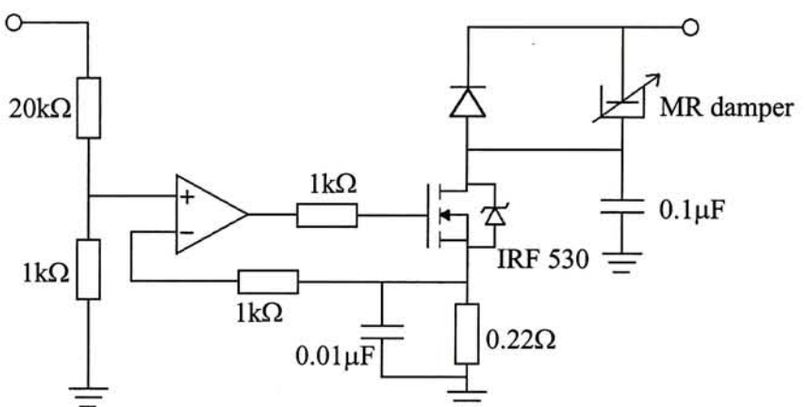
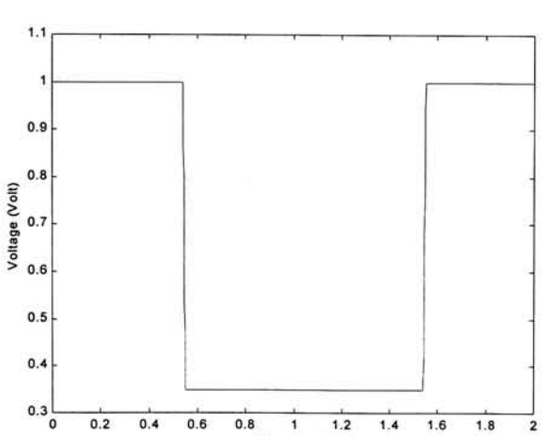
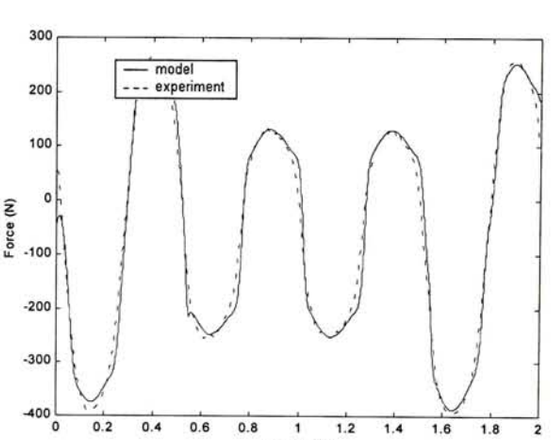


Figure 2.24: Current driver circuit for MR damper

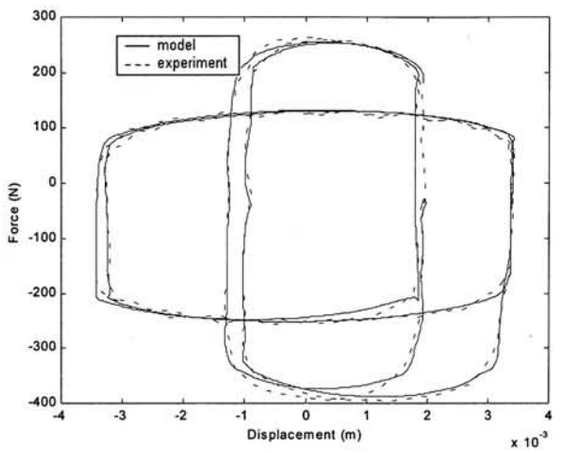
In the first and second tests, the voltage to the damper is changed by a step signal and the damper is excited by a sinusoidal signal at 2 Hz. The voltage changes between 0.35 and 1 volt in the first test while it changes between 0.35 and 2 volts in the second one. For these two cases, the applied voltages are shown in Figure 2.25(a) and Figure 2.26(a).



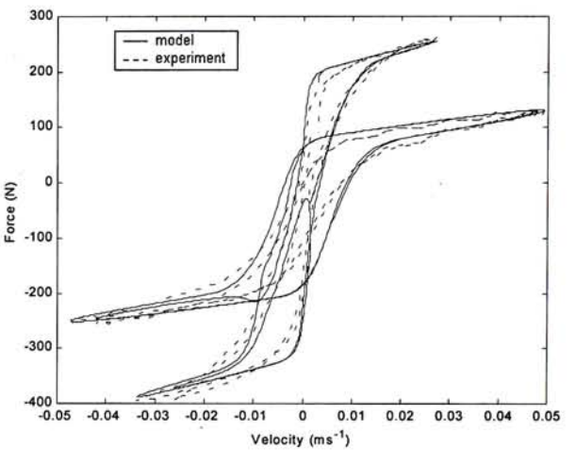
(a) Applied voltage



(b) Force response

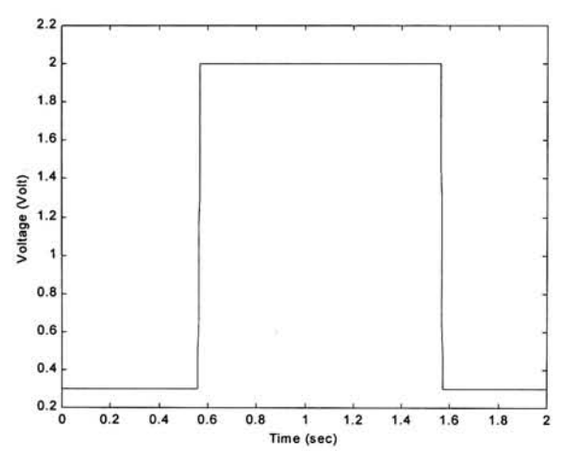


(c) Force-displacement relationship

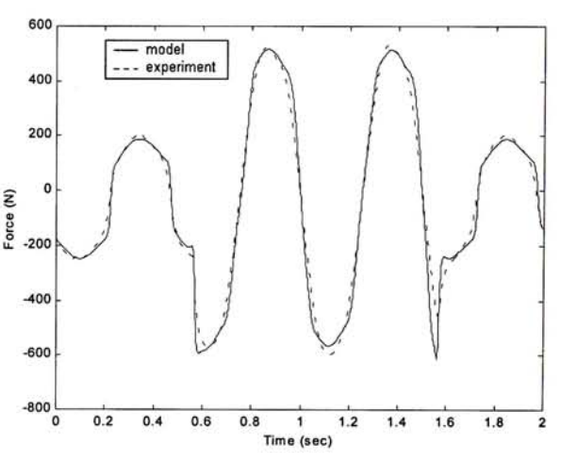


(d) Force-velocity relationship

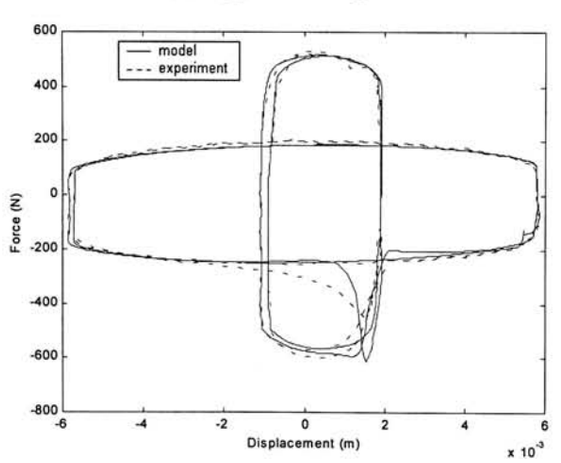
Figure 2.25: First test for the model of the damper



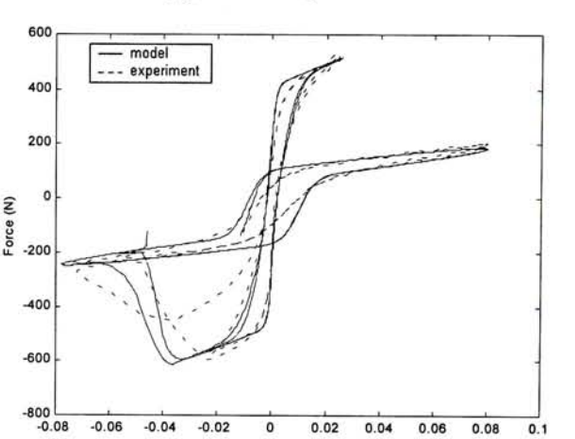
(a) Applied voltage



(b) Force response



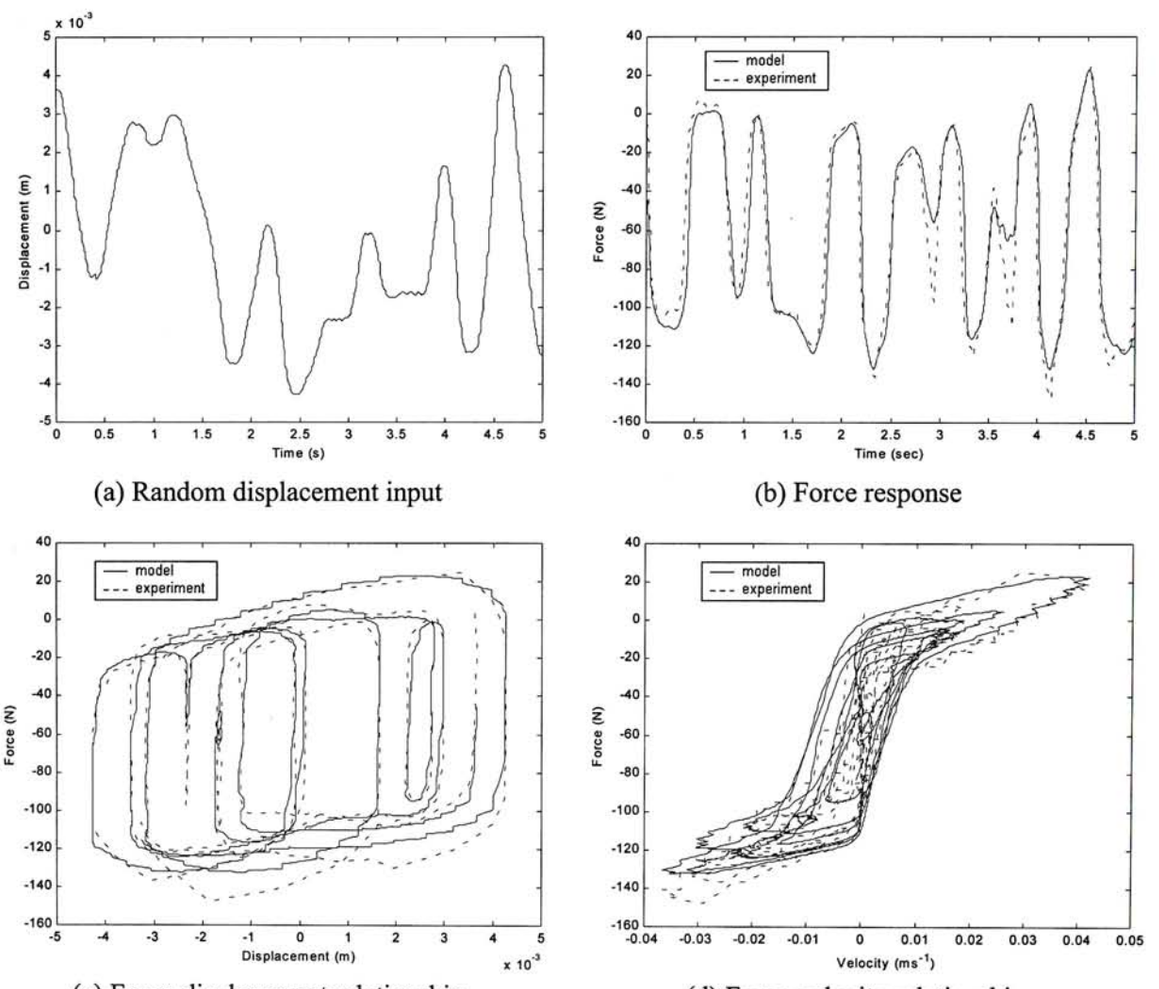
(c) Force-displacement relationship



(d) Force-velocity relationship

Figure 2.26: Second test for the model of the damper

Other plots in Figures 2.25 and 2.26 compare the predicted results to the experimental data for the corresponding input signals. The differences within comparison are quite small in both cases.



(a) Random displacement input

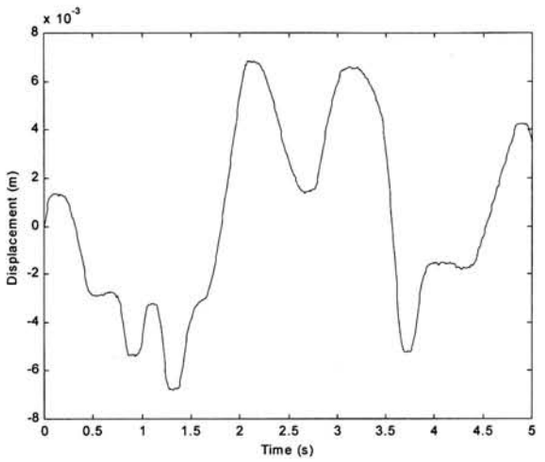
(b) Force response

(c) Force-displacement relationship

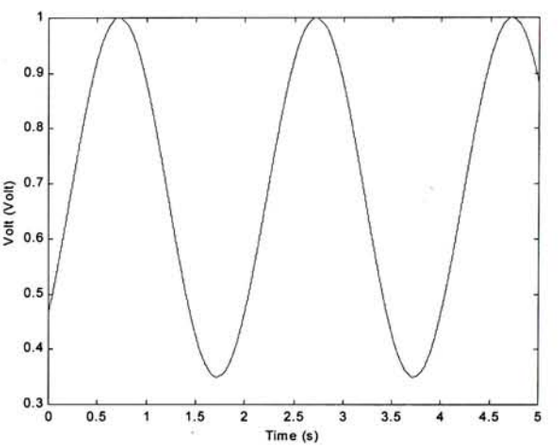
(d) Force-velocity relationship

Figure 2.27: Third test for the model of the damper

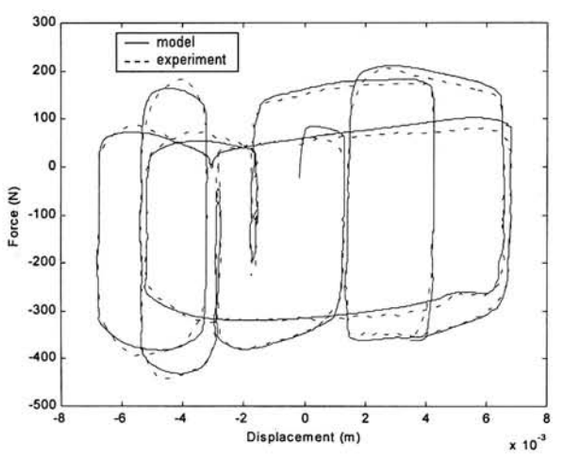
In the third test for the model of the MR damper, the damper is excited with random input signal and the applied voltage is held at zero volts. The displacement record is shown in Figure 2.27(a). The simulated force is compared to the experimental data in Figure 2.27(b), (c) and (d). Also, the model well predicts the behaviour of the MR damper in this case.



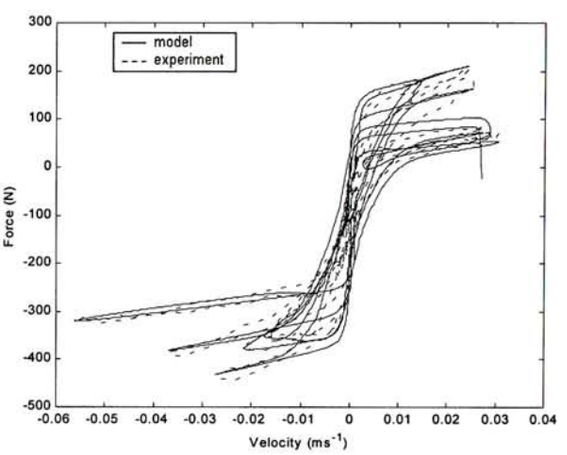
(a) Random displacement input



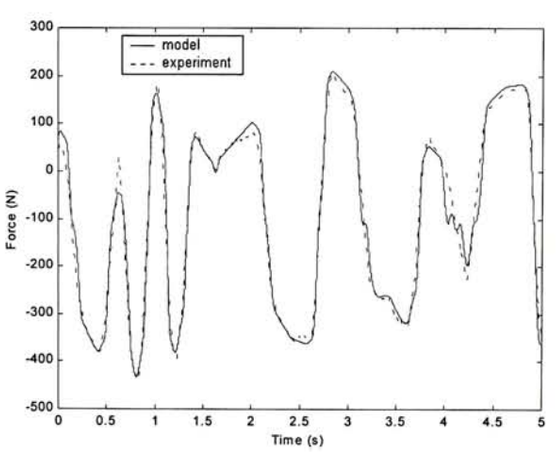
(b) Sinusoidal applied voltage



(c) Force-displacement relationship



(d) Force-velocity relationship



(e) Force response

Figure 2.28: Final test for the model of the damper

For the final verification test, the signal inputted to the shaker is randomized and the voltage applied to the damper is sinusoidal, as shown in Figure 2.28(a) and (b). The

comparison between the predicted model and test data from the real damper is made and the results are shown in Figure 2.28(c), (d) and (e). Again, good agreement is found between the model and the damper.

CHAPTER THREE

SEMI-ACTIVE VIBRATION CONTROL

3.1 Dynamic Modelling of Suspension Systems

Consider the single-degree-of-freedom suspension system shown in Figure 3.1, the equation of motion can be derived as:

$$m_s\ddot{x}_s = -k(x_s - x_b) - c(\dot{x}_s - \dot{x}_b) \tag{3.1}$$

where m_s is the sprung mass

$x_s, \dot{x}_s$ are the vertical displacement and velocity of the sprung mass

k is the stiffness coefficient

$x_b, \dot{x}_b$ are the disturbance and its velocity

c is the damping ratio

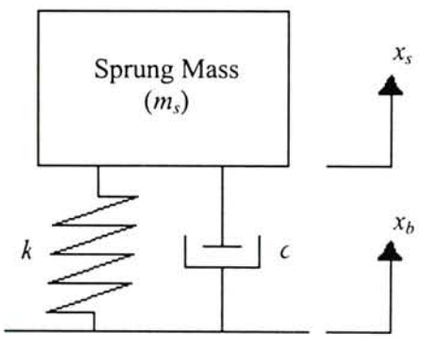


Figure 3.1: Single-degree-of-freedom system

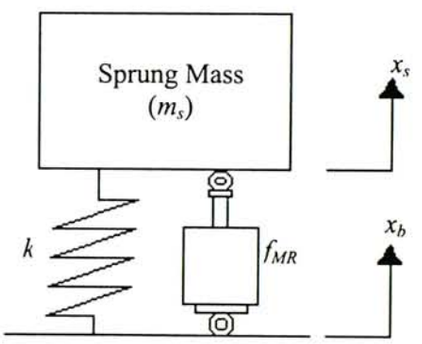


Figure 3.2: Single-degree-of-freedom system with MR damper

With the similar way, we can construct the mathematical model for the one-degree-of-freedom suspension system with MR damper as shown in Figure 3.2. The governing equation of motion is

$$m_s\ddot{x}_s = -k(x_s - x_b) - f_{MR} \tag{3.2}$$

where m_s is the sprung mass

x_s is the vertical displacement of the sprung mass

k is the stiffness coefficient

x_b is the disturbance

f_{MR} is the controllable damping force

3.2 Single-degree-of-freedom (SDOF) Passive Suspension System

3.2.1 Viscous Damper

Considering the model in Figure 3.1, assume the base of the system undergoes harmonic motion, i.e.

$$x_b(t) = Z\sin\omega t \tag{3.3}$$

Eq. (3.1) becomes

$$m_s\ddot{x}_s + c\dot{x}_s + kx_s = kZ\sin\omega t + c\omega Z\cos\omega t = F_0\sin(\omega t - \alpha) \tag{3.4}$$

where $F_0 = Z\sqrt{k^2 + (c\omega)^2}$ and $\alpha = \tan^{-1}\left(-\frac{c\omega}{k}\right)$.

In order to solve for the steady state solution of Eq. (3.4), we consider the equation of motion with harmonic force $F(t) = F_0 e^{i\omega t}$.

$$m_s\ddot{x}_s + c\dot{x}_s + kx_s = F_0 e^{i\omega t} \tag{3.5}$$

The solution for Eq. (3.5) is

$$x_s(t) = Xe^{i\omega t} \tag{3.6}$$

By substituting Eq. (3.6) into Eq. (3.5), the amplitude of the response can be found to be

$$X = \frac{F_0}{(k - m_s\omega^2) + ic\omega}.$$

As a result,

$$X = \frac{F_0}{\left[\left(k - m_s\omega^2\right)^2 + (c\omega)^2\right]^{\frac{1}{2}}} e^{-i\theta} \tag{3.7}$$

where $\theta = \tan^{-1}\left(\frac{c\omega}{k - m_s\omega^2}\right)$

So, the steady state solution of Eq. (3.5) is

$$x_s(t) = \frac{F_0}{\left[\left(k - m_s\omega^2\right)^2 + (c\omega)^2\right]^{\frac{1}{2}}} e^{i(\omega t - \theta)} \tag{3.8}$$

If the excitation force is of the form $F(t) = F_0 \sin \omega t$, then the corresponding steady state solution is given by the imaginary part of Eq. (3.8). So,

$$x_s(t) = \frac{F_0}{\left[\left(k - m_s\omega^2\right)^2 + (c\omega)^2\right]^{\frac{1}{2}}} \sin(\omega t - \theta) \tag{3.9}$$

As a result, the steady state response of the sprung mass described in Eq. (3.4) can be expressed as

$$x_s(t) = \frac{Z\sqrt{k^2 + (c\omega)^2}}{\left[\left(k - m_s\omega^2\right)^2 + (c\omega)^2\right]^{\frac{1}{2}}} \sin(\omega t - \alpha - \theta) \tag{3.10}$$

where $\alpha = \tan^{-1}\left(-\frac{c\omega}{k}\right)$ and $\theta = \tan^{-1}\left(\frac{c\omega}{k - m_s\omega^2}\right)$

Eq. (3.10) can be rewritten as:

$$x_s(t) = X_s \sin(\omega t - \phi) \tag{3.11}$$

where $X_s = \frac{Z\sqrt{k^2 + (c\omega)^2}}{\left[\left(k - m_s\omega^2\right)^2 + (c\omega)^2\right]^{\frac{1}{2}}}$ and $\phi = \theta + \alpha = \tan^{-1}\left[\frac{m_s c\omega^3}{k\left(k - m_s\omega^2\right) + (\omega c)^2}\right]$

The displacement transmissibility amplitude $\frac{X_s}{Z}$ and transmissibility phase ϕ can be expressed as

$$\frac{X_s}{Z} = \left[\frac{k^2 + (c\omega)^2}{\left(k - m_s\omega^2\right)^2 + (c\omega)^2}\right]^{\frac{1}{2}} = \left[\frac{1 + (2\zeta r)^2}{\left(1 - r^2\right)^2 + (2\zeta r)^2}\right]^{\frac{1}{2}} \tag{3.12}$$

$$\phi = \tan^{-1}\left[\frac{2\zeta r^3}{1 + \left(4\zeta^2 - 1\right)r^2}\right] \tag{3.13}$$

where $\zeta = \frac{c}{2\sqrt{m_s k}}$ and $r = \frac{\omega}{\omega_n} = \frac{\omega\sqrt{m_s}}{\sqrt{k}}$

ω_n is the natural frequency of the system. ζ is the damping ratio and r is the frequency ratio.

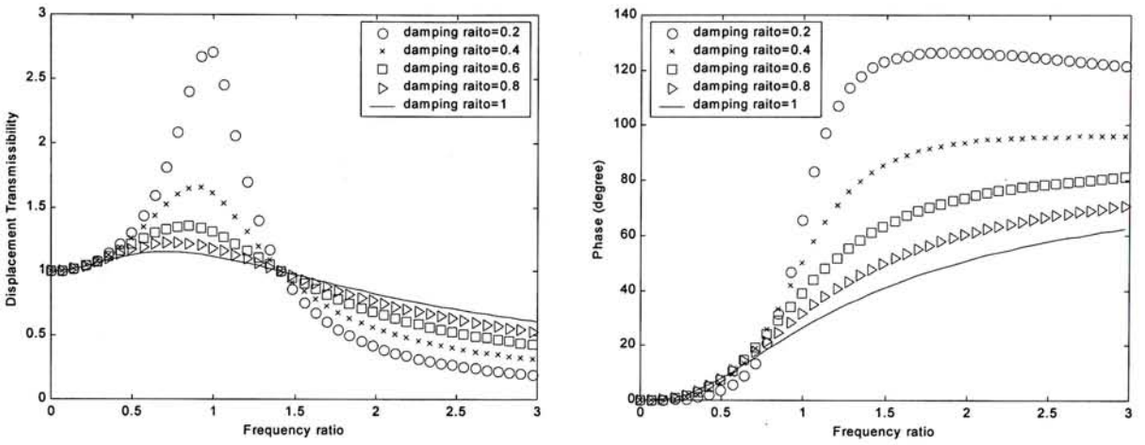
Similarly, the acceleration transmissibility of the system can be found out.

$$\text{acceleration transmissibility} = \frac{X_s'}{Z'} = \left[\frac{1 + (2\zeta r)^2}{\left(1 - r^2\right)^2 + (2\zeta r)^2}\right]^{\frac{1}{2}} \tag{3.14}$$

where X_s' and Z' are the amplitudes of the accelerations of the sprung mass and the base excitation respectively.

It should be noted that the displacement and acceleration transmissibility for the SDOF system using viscous damper are equal. The displacement transmissibility and the phase shift of the SDOF system, if all the elements of the system are passive, are shown in Figure 3.3 for various damping coefficients.

From Figure 3.3(a), it can be seen that at low passive damping, the resonant transmissibility (frequency ratio = 1) is relatively large, while the transmissibility at higher frequency is quite low.



(a) Displacement transmissibility (b) Phase shift

Figure 3.3: Transmissibility and phase for the passive suspension with viscous damper

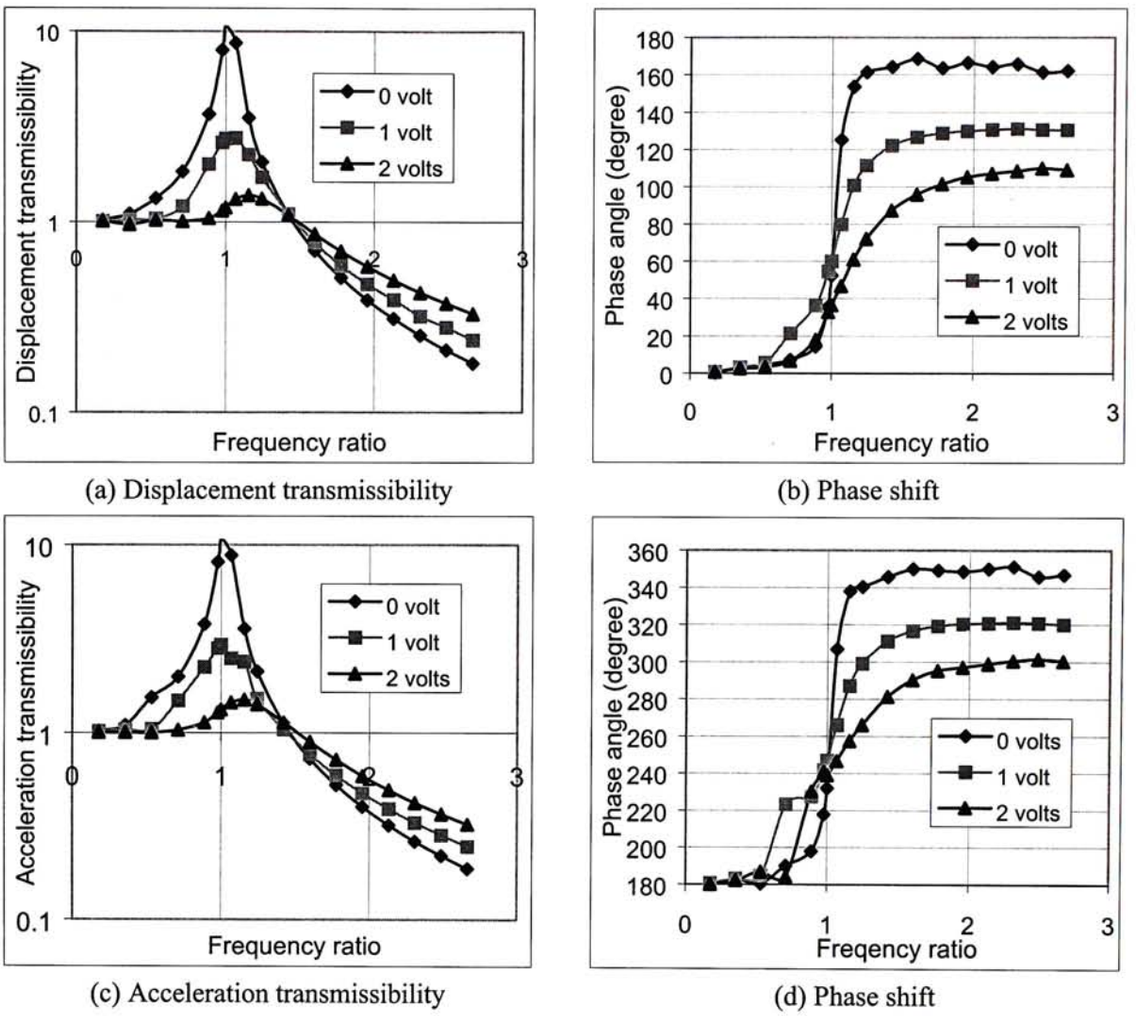
As the damping is increased, the resonant peak is attenuated but isolation is lost at high frequency. This transmissibility plot graphically illustrates the inherent tradeoff between resonance control and high frequency isolation that is associated with the design of passive suspension system.

Also, from Figure 3.3(a), the location of the peak of the transmissibility for the damping ratio 0.2 is almost at unity frequency ratio. But, as the damping ratio is increased, the location of the peak shifts to smaller frequency ratio.

Figure 3.3(b) presents the coupling effect between the base excitation and the motion of the sprung mass. A small phase angle means that the two ends of the damper are strongly coupled and are moving in phase with each other. Increasing damping causes more coupling across the suspension system.

3.2.2 MR Damper

Using the MR damper model studied in the previous chapter, the displacement transmissibility, acceleration transmissibility and phase shifts are found out through simulation. They are shown in Figure 3.4.



(a) Displacement transmissibility

(b) Phase shift

(c) Acceleration transmissibility

(d) Phase shift

Figure 3.4: Transmissibility and phase for the passive suspension with MR damper

In the simulation, the sprung mass is set to be 1500 kg and the stiffness of the spring is 75000 N/m. The base excitation is set to be 0.01 m. As expected, they are similar to those cases in viscous damper. For low frequency, the transmissibilities are higher for low damping (low voltage applied). In this case, 0 volt input causes the lowest damping of MR damper. As the voltage applied is increased, the transmissibility decreases. For higher frequency, lower voltage input (lower damping) has a better isolation.

One interesting thing to note is that the locations of the peaks of those transmissibilities shift to higher frequency ratio as the input voltage increases (larger

damping). This is totally different from the cases for viscous damper. In order to investigate this characteristic, the equivalent damping coefficient c_{eq} is found for each data point. Before determining the energy dissipated in each cycle, the amplitude of relative motion (x_s - x_b) of the damper for the SDOF system should be found. The relative displacements of the damper are shown in Figure 3.5.

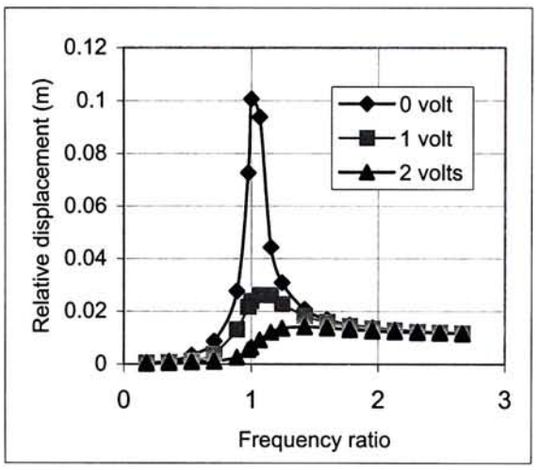


Figure 3.5: Relative displacement of the SDOF system

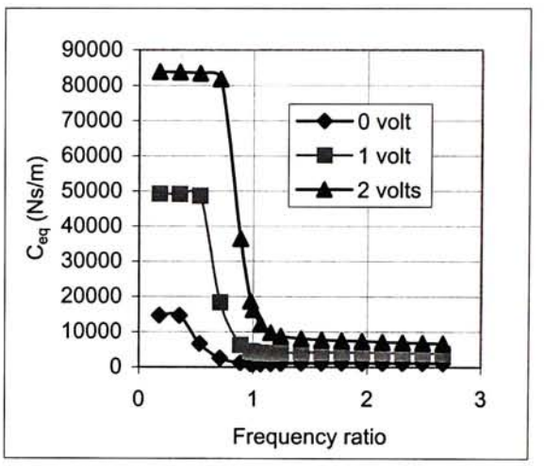


Figure 3.6: Equivalent damping coefficient for each voltage

By using Eq. (2.11), c_{eq} can be calculated by substituting Y by the relative displacement where W can be found by using Eq. (2.8). The plot of these values against frequency ratio for various input voltages are shown in Figure 3.6. The displacement transmissibility can be calculated using Eq. (3.12) with variable damping and frequency. These results are plotted in Figure 3.7 with the plots in Figure 3.4 (a) for the purpose of comparison. It can be seen that the transmissibility from the system simulation is quite close to that calculated from c_{eq}.

In Figure 3.6, the equivalent damping coefficients drop for all voltage cases as the frequency ratio increases although the locations of the drop are different. Referring to Figure 3.5, when c_{eq} remains in high value, the amplitude of relative displacement is very low. That means, the MR fluid in the damper is near pre-yield phase at that time.

When the amplitude of relative displacement is higher, the damping force exceeds the yield force of the MR fluid and the damper operates in the post-yield region. In this phase, the equivalent damping will be much smaller. This illustrates that c_{eq} can change dramatically with the amplitude of the relative displacement.

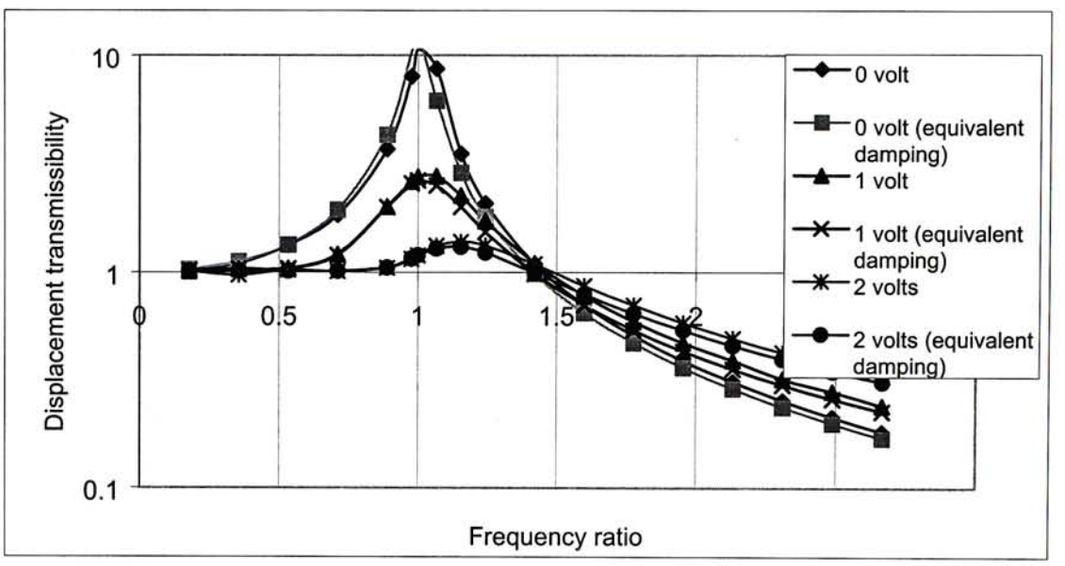


Figure 3.7: Comparison between two transmissibilities of SDOF system

In Figure 3.6, the c_{eq} value drops significantly from the frequency ratio of about 0.8 for 2 volts input while it drops from that of about 0.4 for 0 volt input. That is, for 0 volt case, the coefficient starts to drop in lower frequency ratio. Then, for 2 volts, c_{eq} drops to as low as 9000 Ns/m after the unity frequency ratio and it stays at that level afterward. But, for 0 volt, it can reach the steady value of c_{eq} at around the unity frequency. It is obviously that the c_{eq} for 2 volts starts lately (in the sense of frequency ratio) to decrease and reach the steady value lately. So, in Figure 3.4(a) and (c), the transmissibility for 2 volts input starts to increase in the frequency ratio of about 0.8 and it will not reach the peak at the unity frequency ratio. It will have a peak after the unity frequency ratio as there still exists significant drop of c_{eq} for 2 volts case at the unity frequency ratio.

From Figure 3.3(a), it should be reminded that the transmissibility at resonance increases significantly with the decrease of damping. That is why sudden damping drop can increase the transmissibility.

3.3 Single-degree-of-freedom (SDOF) Semi-active Suspension System

3.3.1 Ideal Skyhook Control

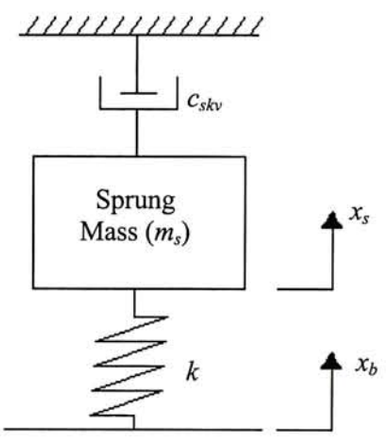


Figure 3.8: SDOF system with skyhook configuration

The skyhook damper configuration attempts to eliminate the tradeoff between resonance control and high frequency isolation common to passive suspensions. Considering the arrangement in Figure 3.8, the damper is connected to an inertial reference in the sky. Clearly, this arrangement is fictitious. The reason is, for this configuration to be implemented, the damper would have to be connected to a reference point which is fixed with respect to the ground but can move with the vehicle. Obviously, such a suspension mounting point does not exist. The end goal of skyhook control is not to physically implement this system but to command a controllable damper to cause the system to respond in similar manner to this ideal system. In this section, the

ideal system is considered in order to present the advantage of such system over the passive one.

The motion equation of ideal skyhook system is

$$m_s\ddot{x}_s + c_{sky}\dot{x}_s + k(x_s - x_b) = 0 \tag{3.15}$$

If the base is under harmonic motion,

$$x_b(t) = Z\sin\omega t \tag{3.16}$$

Eq. (3.15) becomes

$$m_s\ddot{x}_s + c_{sky}\dot{x}_s + kx_s = kZ\sin\omega t \tag{3.17}$$

From Eq. (3.9),

$$x_s(t) = \frac{kZ}{\left[\left(k - m_s\omega^2\right)^2 + \left(c_{sky}\omega\right)^2\right]^{\frac{1}{2}}}\sin(\omega t - \phi) \tag{3.18}$$

where $\phi = \tan^{-1}\left(\dfrac{c_{sky}\omega}{k - m_s\omega^2}\right)$

Eq. (3.18) can be rewritten as:

$$x_s(t) = X_s\sin(\omega t - \phi) \tag{3.19}$$

where $X_s = \dfrac{kZ}{\left[\left(k - m_s\omega^2\right)^2 + \left(c_{sky}\omega\right)^2\right]^{\frac{1}{2}}}$ and $\phi = \tan^{-1}\left(\dfrac{c_{sky}\omega}{k - m_s\omega^2}\right)$

The displacement transmissibility amplitude $\dfrac{X_s}{Z}$ and transmissibility phase ϕ can be expressed as

$$\frac{X_s}{Z} = \frac{k}{\left[\left(k - m_s\omega^2\right)^2 + \left(c_{sky}\omega\right)^2\right]^{\frac{1}{2}}} = \frac{1}{\left[\left(1 - r^2\right)^2 + \left(2\zeta r\right)^2\right]^{\frac{1}{2}}} \tag{3.20}$$

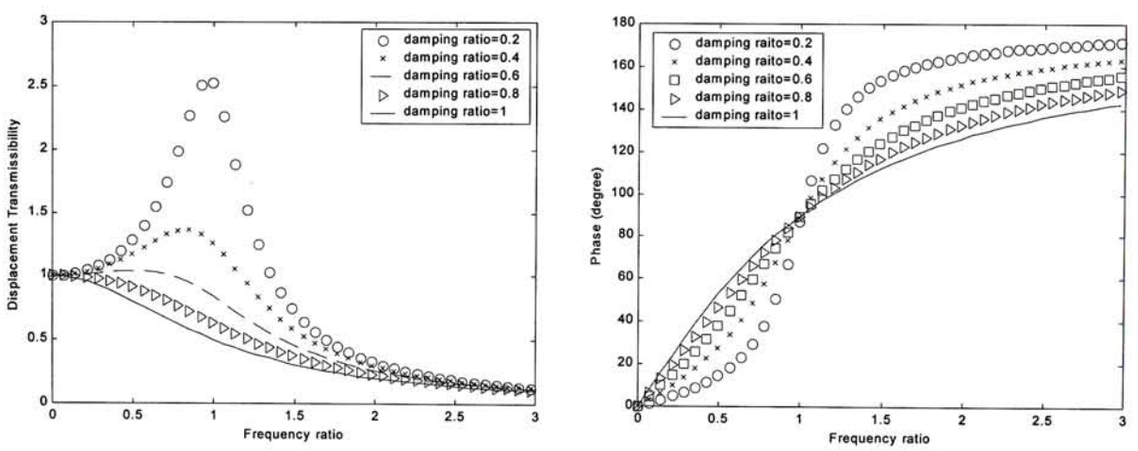
$$\phi = \tan^{-1}\left[\frac{2\zeta r}{1-r^2}\right] \tag{3.21}$$

where $\zeta = \frac{c_{sky}}{2\sqrt{m_s k}}$ and $r = \frac{\omega}{\omega_n} = \frac{\omega\sqrt{m_s}}{\sqrt{k}}$. ζ is the damping ratio and r is the frequency ratio.

Similarly, the acceleration transmissibility of the system can be found out.

$$\text{acceleration transmissibility} = \frac{1}{\left[\left(1-r^2\right)^2 + \left(2\zeta r\right)^2\right]^{\frac{1}{2}}} \tag{3.22}$$

The transmissibility of the skyhook system, if all the elements of the system are passive, are shown in Figure 3.9 for various damping coefficients.



(a) Displacement transmissibility (b) Phase shift

Figure 3.9: Transmissibility and phase for the ideal semi-active suspension

From Figure 3.9, as the damping increases, the advantage of using this control becomes more obvious. Using the same damping ratio, this kind of suspension can have displacement transmissibility below unity at all frequency while the passive one cannot do this at frequency ratio less than $\sqrt{2}$ [33]. The compromise between resonance control and isolation at high frequency does not exist for such system. With sufficiently large

damping ratio, the resonant peak and amplitude at high frequency can be eliminated across the whole frequency range.

3.3.2 Semi-active Skyhook Control

In the previous section, it can be proved that ideal skyhook can provide a better isolation performance than the passive one. As mentioned earlier, this skyhook control configuration is ideal in nature. But, we can use controllable damper to mimic the action of this ideal skyhook control. Then, the system changes to semi-active type but the characteristics of good performance can still be captured.

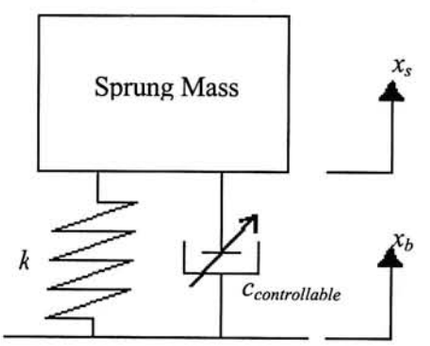


Figure 3.10: Semi-active suspension system

Now, the means of modulating the damper such that it emulates a skyhook damper must be determined. We first define the velocity of the sprung mass relative to the base ($\dot{x}_{sb}$) to be positive when the sprung mass and the base are separating (i.e., $\dot{x}_s$ is greater than $\dot{x}_b$). Now, the sprung mass is moving upwards with a positive velocity. If we consider the force that is applied by the skyhook damper to the sprung mass in Figure 3.8, we notice that it is in the negative $\dot{x}_s$ direction, or

$$F_{sky} = -c_{sky}\dot{x}_s \tag{3.23}$$

where F_{sky} is the skyhook force.

Next, we need to determine if the semi-active damper is able to provide the same force. If the sprung mass and the base are separating, the semi-active damper is in tension. Thus, the force applied to the sprung mass is in the negative $\dot{x}_s$ direction, or

$$F_{controllable} = -c_{controllable}\dot{x}_{sb} \tag{3.24}$$

where $F_{controllable}$ is the force applied to the sprung mass.

Since we are able to generate a force in the proper direction, the only requirement to match the skyhook suspension is

$$c_{controllable} = c_{sky} \times \frac{\dot{x}_s}{\dot{x}_{sb}} \tag{3.25}$$

To summarize, if $\dot{x}_s$ and $\dot{x}_{sb}$ are positive, $c_{controllable}$ should be defined as in Eq. (3.25).

Next, the sprung mass and the base are still separating but the sprung mass is moving downwards with a negative velocity. In the ideal skyhook configuration, the damping force will now be applied in the upward, or positive direction. In the semi-active configuration, however, the damper is still in tension. Then, the damping force will still be applied in the downward, or negative direction. Since the semi-active damping force cannot possibly be applied in the same direction as the skyhook damping force, the best that can be achieved is to minimize the damping force. Ideally, the semi-active damper is desired to be set so that there is no damping force. However, in reality, there is some inherent damping force present and it is not in the same direction as the skyhook damping force. Thus, if $\dot{x}_{sb}$ is positive and $\dot{x}_s$ is negative, we need to minimize the semi-active damping force.

We can apply the same simple analysis to the other two combination of $\dot{x}_s$ and $\dot{x}_{sb}$, resulting in the following semi-active skyhook control policy:

$$\begin{cases} F_{sa} = -c_{sky}\dot{x}_s & \dot{x}_s\dot{x}_{sb} \geq 0 \\ F_{sa} = 0 & \dot{x}_s\dot{x}_{sb} < 0 \end{cases} \tag{3.26}$$

where F_{sa} is the semi-active skyhook damping force

Eq. (3.26) implies that when the relative velocity across the damper and the sprung mass absolute velocity have the same sign, a damping force proportional to the absolute velocity is desired. Otherwise, the minimal amount of damping is good enough.

3.4 Semi-active Robust Control Development

In this study, a semi-active vibration control system is proposed, which block diagram is shown in Figure 3.11. The plant is a SDOF spring-mass system. The control part consists of two nested controllers. The outer controller, which is sliding mode controller, generates the desired controlled force according to the response of the suspension system while the inner controller adjusts the voltage level to track the desired force generated by the outer controller. These controllers will be discussed in the following two sections.

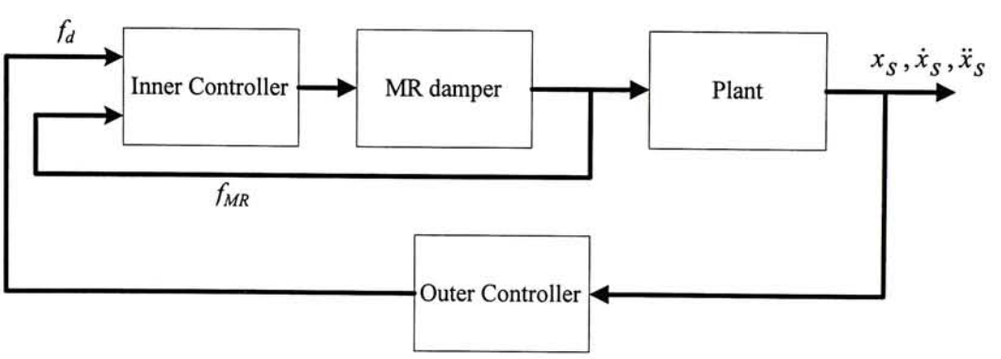


Figure 3.11: Block diagram of the semi-active control system

3.5 Sliding Mode Control

A sliding mode controller is used as the outer controller for the semi-active control system. The major advantages of employing this robust control technique are that the algorithm can be synthesized for the nonlinear semi-active system adequately, and that the system can be designed to be robust with respect to unmodeled dynamics, system variations and external disturbances.

In practice, the sprung mass varies by the loading conditions such as the number of riding persons and payloads. Therefore, we consider that parameter perturbations of the sprung mass exist in the system. Assume the possible bound of the mass can be expressed as follows:

$$m_s = m_{so} + \Delta m_s \text{ and } |\Delta m_s| \le 0.2 m_{so} \tag{3.27}$$

where m_{so} represents the nominal mass and Δm_s is uncertain part. The uncertainty ratio 0.2 is chosen here for the purpose of discussion.

First, the sliding surface is defined as

$$S = \dot{e} + \lambda e \tag{3.28}$$

where $e = x_s - x_{ref}$.

x_{ref} is the displacement of the sprung mass in the reference model. The reference model used for this suspension system is the ideal skyhook system. The configuration has been mentioned in the previous section. It has been shown that vibration across the broad frequency range can be significantly reduced. Therefore, the performance of the reference model can be treated as the desired one for suspension system while a large damping ratio is chosen. In this study, the damping coefficient of the reference model is

35000 N/(ms^{-1}). The controller is designed so as to compensate the difference of responses between the system and the reference model.

Further, the error between the estimated nominal value and the real value is assumed to be bounded by known β:

$$\frac{1}{\beta} \le \frac{\frac{1}{m_{so}}}{\frac{1}{m_s}} \le \beta \Rightarrow \frac{1}{\beta} \le \frac{m_s}{m_{so}} \le \beta \Rightarrow \frac{1}{\beta} \le 1 + \frac{\Delta m_s}{m_{so}} \le \beta \tag{3.29}$$

$1 + \frac{\Delta m_s}{m_{so}}$ is maximum when $\Delta m_s = 0.2 m_{so}$ while it is minimum when $\Delta m_s = -0.2 m_{so}$. So, β can be chosen to be 1.25.

In order to ensure the state will move toward and reach the sliding surface, a sliding condition must be defined. The sliding condition proposed [34] is

$$S\dot{S} \le -\varphi |S| \tag{3.30}$$

where φ is a strictly positive constant. It constrains trajectories to point towards the sliding surface, as illustrated in Figure 3.12. In particular, once on the surface, the system trajectories remain on the surface, i.e. $S = 0$.

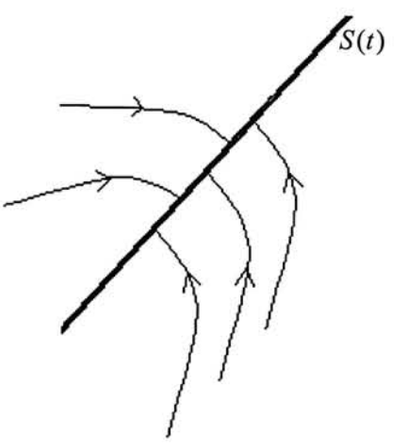


Figure 3.12: Sliding condition

From Eqs. (3.2) and (3.28),

$$\begin{aligned}\dot{S} &= \ddot{e} + \lambda\dot{e} \\ &= \ddot{x}_s - \ddot{x}_{ref} + \lambda\dot{e} \\ &= -\frac{k}{m_s}(x_s - x_0) - \frac{f_{MR}}{m_s} - \ddot{x}_{ref} + \lambda\dot{e}\end{aligned} \tag{3.31}$$

The best approximation u_o of a control law that would achieve $\dot{S} = 0$ is thus

$$u_o = -m_{so}\left(\frac{k}{m_{so}}x_s - \frac{k}{m_{so}}x_0 - \lambda\dot{e} + \ddot{x}_{ref}\right) \tag{3.32}$$

In order to satisfy sliding condition, despite mass uncertainty, a term discontinuous across the surface is added to the expression u_o. The desired control force f_d can be expressed as

$$f_d = u_o - K\,\mathrm{sgn}(S) \tag{3.33}$$

Eq. (3.33) can be expressed as

$$f_d = -m_{so}\left[u_o' - K'\,\mathrm{sgn}(S)\right] \tag{3.34}$$

where $u_o' = -\dfrac{u_o}{m_{so}}$ and $K' = -\dfrac{K}{m_{so}}$

Now, the range of the switching gain K' to make the system stable is to be found.

Eq. (3.30) can be interpreted as

$$\begin{cases}\dot{S} \le -\varphi & \text{when } S \ge 0 \\ \dot{S} > \varphi & \text{when } S < 0\end{cases} \tag{3.35}$$

And, Eq. (3.31) gives the following by putting f_{MR} equal to f_d:

$$\dot{S} = -\frac{k}{m_s}(x_s - x_0) + \frac{m_{so}}{m_s}\left[u_o' - K'\,\mathrm{sgn}(S)\right] - \ddot{x}_{ref} + \lambda\dot{e}$$

$$
\begin{aligned}
&= -\frac{k}{m_s}(x_s - x_0) + \frac{m_{so}}{m_s}\left[\frac{k}{m_{so}}(x_s - x_0)\right] \\
&\quad -\frac{m_{so}}{m_s}[K'\operatorname{sgn}(S)] + \left(1 - \frac{m_{so}}{m_s}\right)\left(-\ddot{x}_{ref} + \lambda\dot{e}\right)
\end{aligned} \tag{3.36}
$$

As a result,

$$
\dot{S} = -\frac{m_{so}}{m_s}[K'\operatorname{sgn}(S)] + \left(1 - \frac{m_{so}}{m_s}\right)\left(-\ddot{x}_{ref} + \lambda\dot{e}\right) \tag{3.37}
$$

From Eq. (3.37), for $S \geq 0$, Eq. (3.35) becomes

$$
-\frac{m_{so}}{m_s}K' + \left(1 - \frac{m_{so}}{m_s}\right)\left(-\ddot{x}_{ref} + \lambda\dot{e}\right) \leq -\varphi
$$

$$
\Rightarrow K' \geq \frac{m_s}{m_{so}}\varphi + \left(\frac{m_s}{m_{so}} - 1\right)\left(-\ddot{x}_{ref} + \lambda\dot{e}\right) \tag{3.38}
$$

Similarly, for $S < 0$,

$$
\frac{m_{so}}{m_s}K' + \left(1 - \frac{m_{so}}{m_s}\right)\left(-\ddot{x}_{ref} + \lambda\dot{e}\right) > \varphi
$$

$$
\Rightarrow K' > \frac{m_s}{m_{so}}\varphi - \left(\frac{m_{so}}{m_s} - 1\right)\left(-\ddot{x}_{ref} + \lambda\dot{e}\right) \tag{3.39}
$$

Combining two cases from Eq. (3.38) and Eq. (3.39),

$$
\begin{aligned}
K' &\geq \left|\left(\frac{m_s}{m_{so}} - 1\right)\left(-\ddot{x}_{ref} + \lambda\dot{e}\right)\right| + \frac{m_s}{m_{so}}\varphi \\
&= \left|\frac{m_s}{m_{so}} - 1\right|\left|-\ddot{x}_{ref} + \lambda\dot{e}\right| + \frac{m_s}{m_{so}}\varphi
\end{aligned} \tag{3.40}
$$

$$
\Rightarrow K' \geq (\beta - 1)\left|-\ddot{x}_{ref} + \lambda\dot{e}\right| + \beta\varphi \tag{3.41}
$$

From Eq. (3.32), the right hand side of Eq. (3.41) becomes

$$(\beta-1)\left|-\ddot{x}_{ref}+\lambda\dot{e}\right|+\beta\varphi=(\beta-1)\left|u_o'-\frac{k}{m_{so}}x_s+\frac{k}{m_{so}}x_0\right|+\beta\varphi$$

$$\leq(\beta-1)|u_o'|+(\beta-1)\left|\frac{k}{m_{so}}x_s\right|+(\beta-1)\left|\frac{k}{m_{so}}x_0\right|+\beta\varphi$$

$$=\beta\left[\left(1-\frac{1}{\beta}\right)\left(\frac{k}{m_{so}}|x_s|+\frac{k}{m_{so}}|x_o|+|u_o'|\right)+\varphi\right] \tag{3.42}$$

Using the above controller, the desired controlled force which satisfies the sliding mode condition can be found out. It is obvious to see that the controller given by Eq. (3.42) is designed in an active control manner. Figure 3.13 show the structure of the sliding mode active suspension system using the reference model.

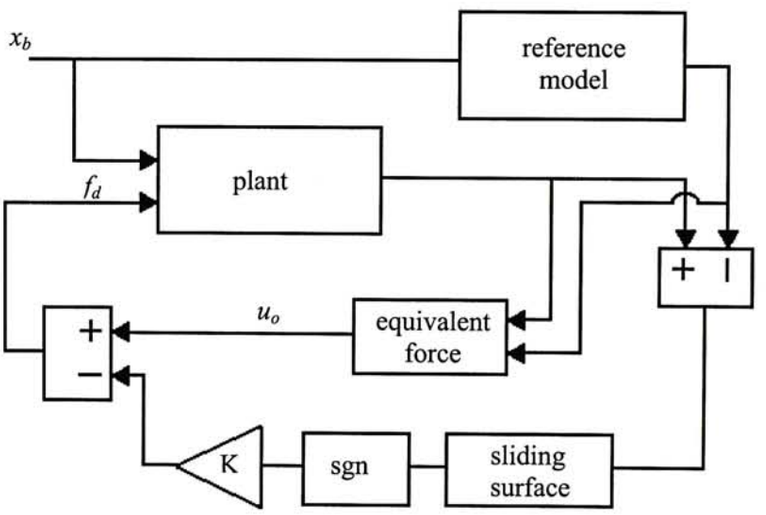


Figure 3.13: Structure of the sliding mode active suspension system

3.6 Semi-active Damper Control

The previous section derives the controlled force outputted from the outer controller. However, MR damper is a semi-active device which cannot generate force

arbitrarily as an active actuator. The response of the MR damper is dependent on the relative displacement and velocity at the point of attachment of the MR damper. So, the best we can do, when the desired force is aimed at adding energy to the system, is to "turn off" the damper. Even the desired force is dissipating energy, the force generated by the MR damper cannot be commanded, but the voltage v applied to the current driver of the damper can be directed controlled. So, a semi-active damper control is used to deal with these two issues.

3.6.1 On-off Control

In this control algorithm, the MR damper will only be turned on (applied with 2 volts) or turned off (no applied voltage). No intermediate voltage will be applied.

The control algorithm can be described as follows. When the MR damper is providing the desired optimal force, the voltage applied to the damper should remain at the present level. If the magnitude of the force produced by the damper is smaller than that of the desired optimal force and the two forces have same sign, the voltage applied to the damper is increased to the maximum level so as to increase the force produced by the damper to match the desired control force. Otherwise, the commanded voltage is set to zero. The algorithm for selecting the voltage signal is graphically represented in Figure 3.14 and can be mathematically stated [6] as

$$v = V_{\max} H((f_d - f_{MR}) f_{MR}) \tag{3.43}$$

where $V_{\max}$ is the maximum voltage to the damper
$H(\cdot)$ is the Heaviside step function

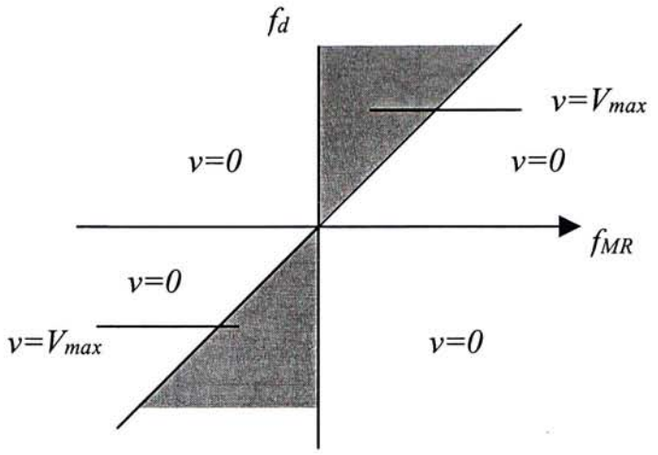


Figure 3.14: Graphical representation of the on-off control

3.6.2 Continuous-state Control

It was proposed [35] that a simple feedback control strategy could linearise the response of the smart fluid damper. To induce the MR damper to generate approximately the corresponding desired control force f_d, the command signal v is selected as follows. Figure 3.15 shows the method in block diagram .

The damping force of MR damper is fed back with a feedback gain B and compared to the desired force. The resulting error is scaled using a proportional gain G. Only when the direction of damping force and the error having the same direction can enable the controller function. This ensures the damper cannot generate energy to the structural system. So, a sign correction is required. If they have different sign, the command voltage signal is set to be zero. The corrected control signal is then saturated between the maximum and minimum voltages. The values of G and B are determined by a trial and error method.

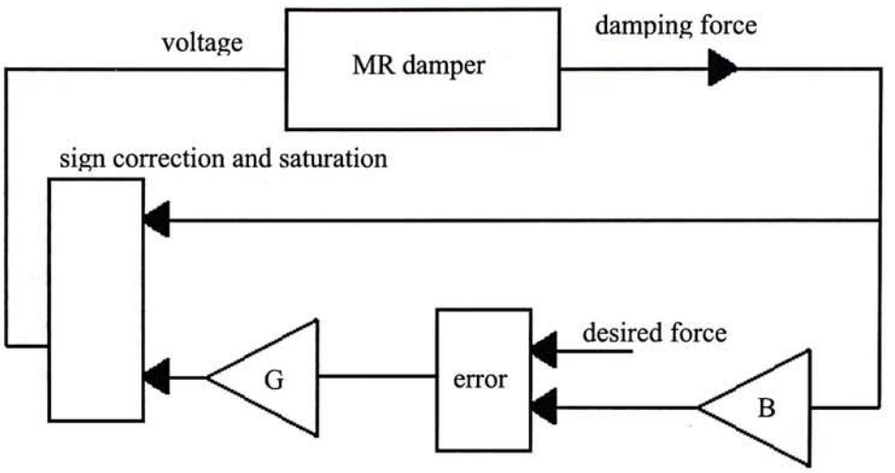


Figure 3.15: Structure of the continuous-state control

The algorithm for selecting the command signal can be stated as

$$\begin{aligned} &\text{if} \quad G(f_d - Bf_{MR})\text{sgn}(f_{MR}) > V_{\max} \\ &\qquad v = V_{\max} \\ &\text{else if} \quad G(f_d - Bf_{MR})\text{sgn}(f_{MR}) < V_{\min} \\ &\qquad v = V_{\min} \\ &\text{else} \\ &\qquad v = G(f_d - Bf_{MR})\text{sgn}(f_{MR}) \end{aligned} \tag{3.44}$$

where V_{max} is the max voltage to the damper

V_{min} is the minimum voltage to the damper (i.e. 0 volt)

3.6.3 Comparison Between On-off and Continuous-state Controller

In order to look for the performance of the damper control algorithms, different kinds of displacement and desired force are inputted to the damper model for inspection. In the first case, the displacement of the damper and the desired damping force are set to be sinusoidal. The magnitude and the frequency of the excitation are 0.01 m and 2 Hz. The desired force is set to be 526.38 N at the same frequency. In the second case, both the displacement of the damper and the desired damping force are randomized under uniform distribution.

Table 3.1: Tracking error of the damping force

	On-off Control	Continuous Control
Error (sinusoidal/random)	34.15 N / 313.31 N	34.05 N / 313.26 N
Voltage (sinusoidal/random)	1.112 V / 0.6630 V	0.7204 V / 0.5556 V

Using the quantitative method to compare the performance of two controllers, the root-mean-square values of error between the damping force and desired one, and corresponding voltage supplied to the damper are shown in Table 3.1. It can be seen that the power needed to operate the continuous controller is less than that for the on-off one with similar performance.

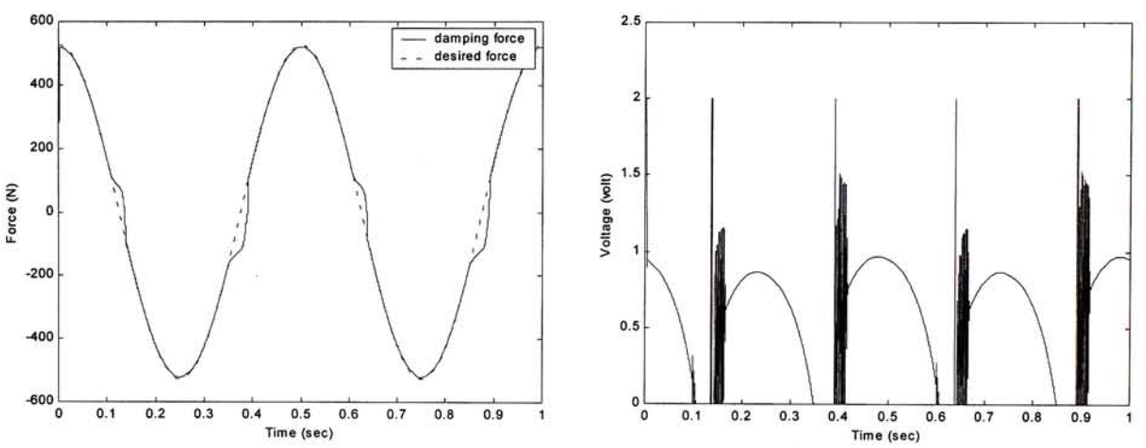


Figure 3.16: First test for the damper controller

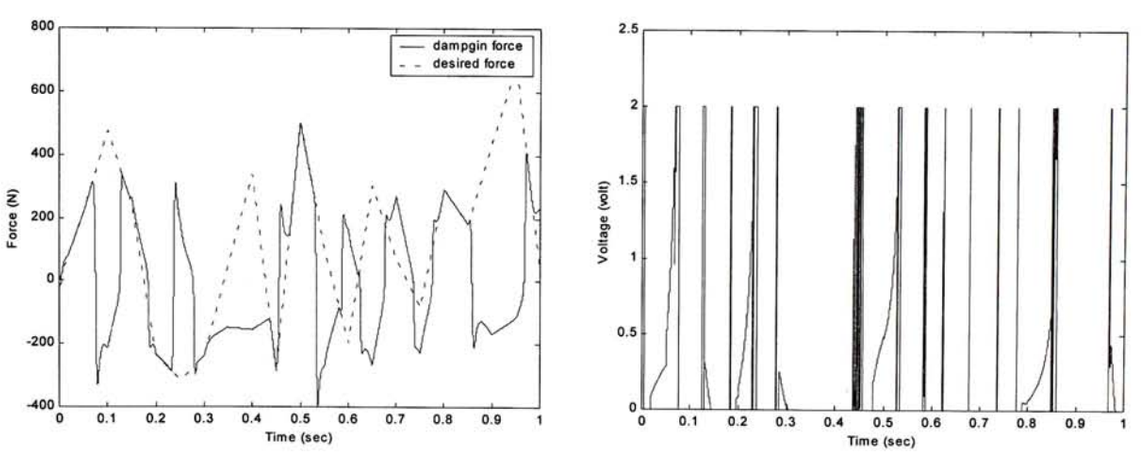


Figure 3.17: Second test for the damper controller

Figure 3.16 presents the performance of the continuous-state controller and the voltage applied to the damper in the first case. It is clearly observed that the damping force tracks well to the desired force by applying control input. For the second case, the performance is shown in Figure 3.17. In these two tests, the values of G and B are set to be 0.021 and 1 respectively.

Within some intervals, the controller tracks the desired force not very well. This happens when the desired force is not in the same direction with the actual damping force which is related to the direction of the velocity. Observing Figures 3.17 and 3.18, the direction of the damping force and velocity is the same. When the direction of desired force is not same as that of velocity, it is impossible for the damper to track it. However, in general, the controller can function well in force tracking under random displacement excitation and random desired force.

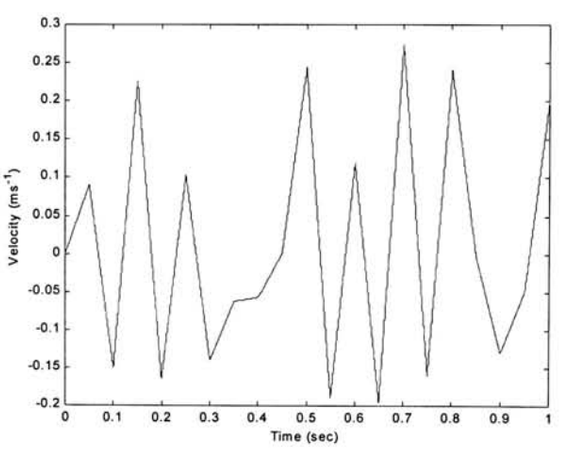


Figure 3.18: Corresponding velocity of MR damper in second test

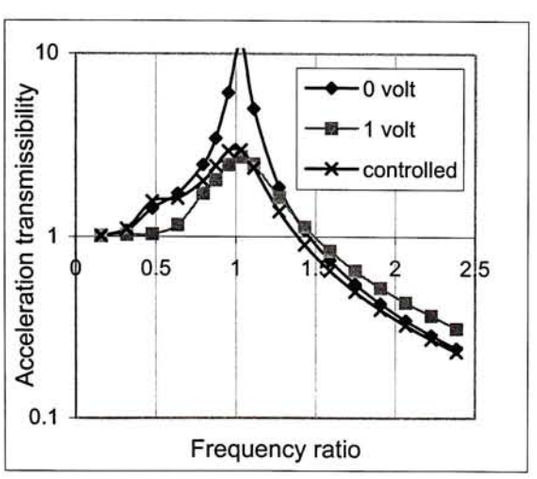
Thus, in the following vibration control simulation study, the inner controller used is the better one within these two - continuous-state controller.

CHAPTER FOUR

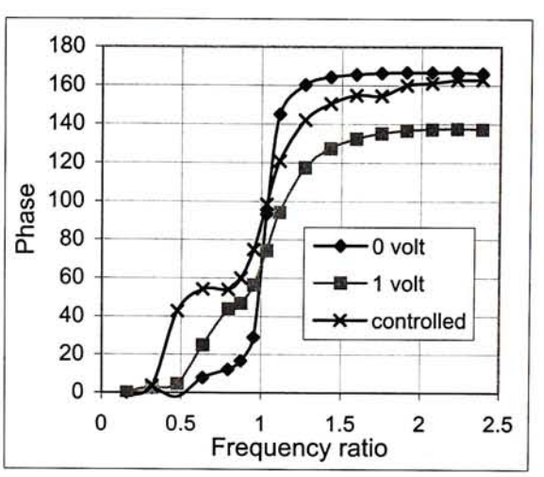
SIMULATION STUDIES

4.1 Transmissibility

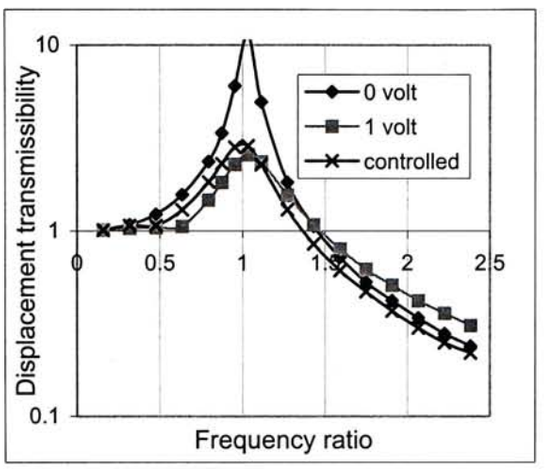
In this section, the performance of the robust vibration control of the SDOF MR suspension system is evaluated through the transmissibility analysis. The nominal parameters used for these simulations are m_{so} = 1500 kg, k = 75000 N/m and Δm_s = -300 kg. In Figure 4.1, the controlled voltage to the damper is constraint between the 0 and 1 volt. In Figure 4.2, the maximum voltage to the damper model is bounded by 2 volts. In both cases, it shows that the isolation performances of the controlled systems are better than that of the system with no voltage applied. Comparing with those figures, one should note that the transmissibilities (both acceleration and displacement) of the controlled system in Figure 4.2 are lower than that of the controlled one in Figure 4.1. So, in the following simulation studies with different base excitations, the maximum voltage to the damper is set to be 2 volts.



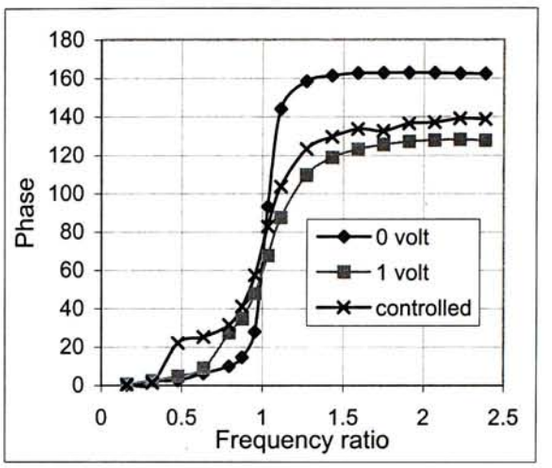
(a) Acceleration transmissibility



(b) Phase shift

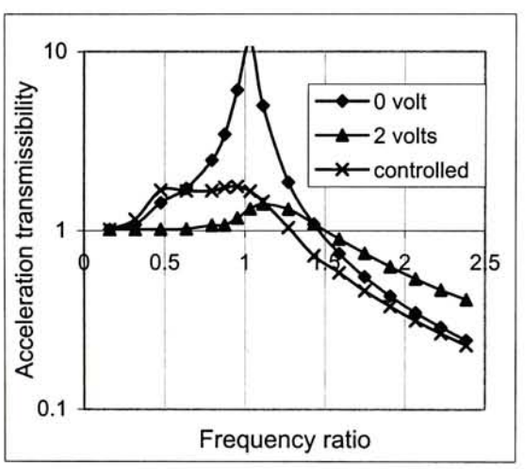


(c) Displacement transmissibility

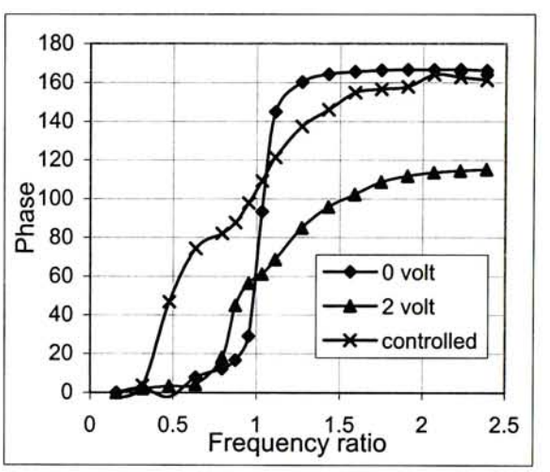


(d) Phase shift

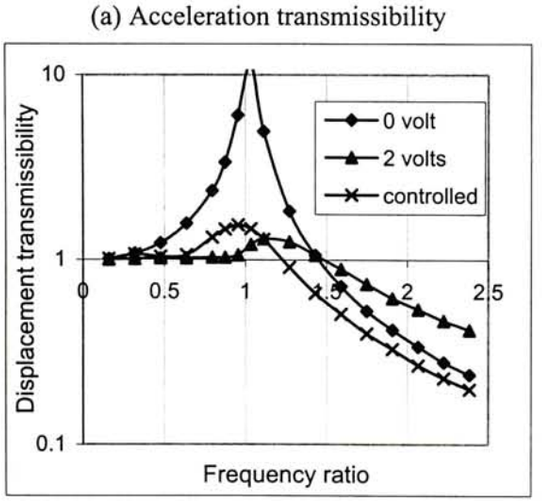
Figure 4.1: Transmissibility of the controlled system with maximum input 1 volt



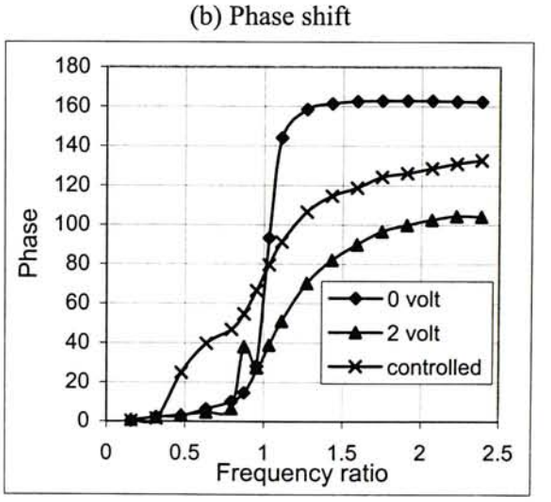
(a) Acceleration transmissibility



(b) Phase shift



(c) Displacement transmissibility



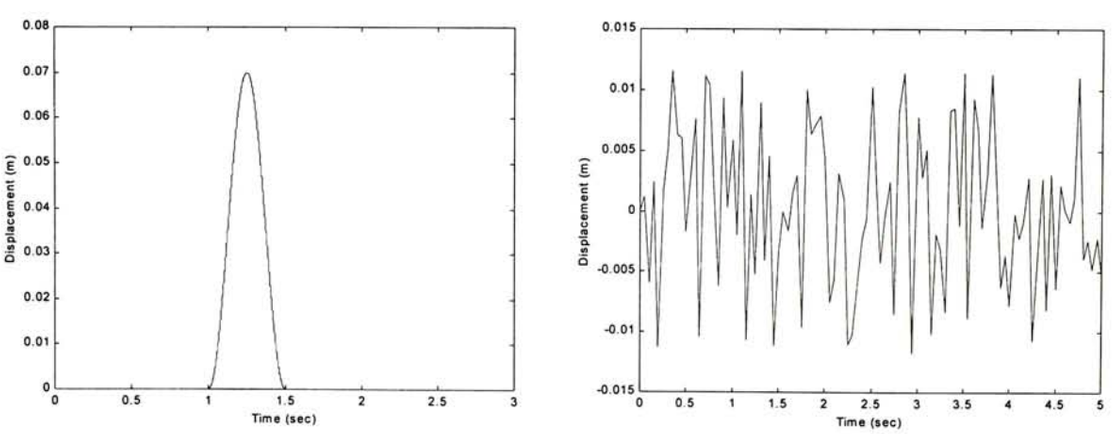
(d) Phase shift

Figure 4.2: Transmissibility of the controlled system with maximum input 2 volts

Also, in both cases, the acceleration transmissibilities of the controlled system are worse than those of uncontrolled ones at some frequency ratio. This is due to the dynamic characteristic of the adopted sliding mode controller. Since there is no acceleration component in the sliding surface in Eq. (3.28), the control mainly suppresses the motion of the sprung mass with displacement and velocity. However, in general, the controllers are still quite effective. This can be shown in the next section.

4.2 Different Base Excitations

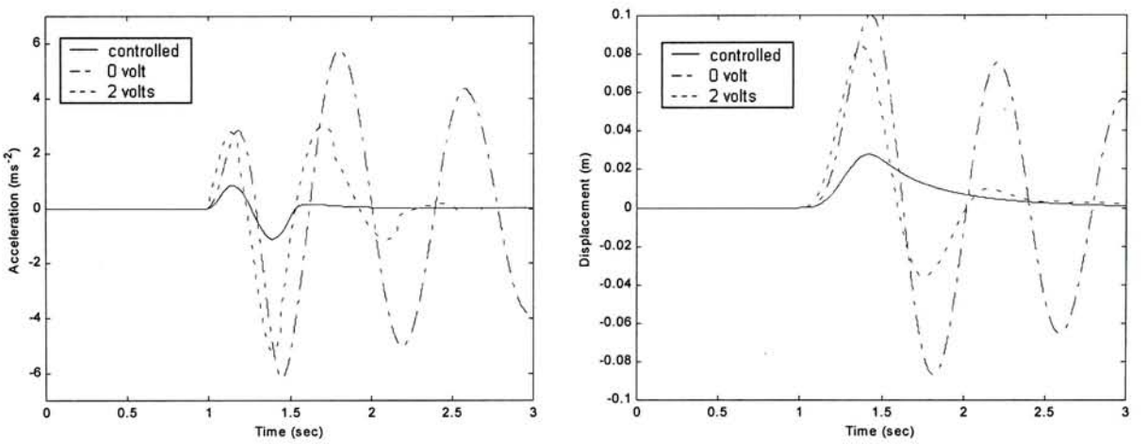
In this section, the performances of the SDOF suspension system with MR damper under two types of road excitations are evaluated through computer simulation. These two excitations are shown in Figure 4.3. Then, the results will be examined in time and frequency domain. The nominal parameters used for these simulation are same as those used in the previous section.



(a) Bump input (b) Random input

Figure 4.3: Two displacement excitations to the system for simulations

4.2.1 Bump Input

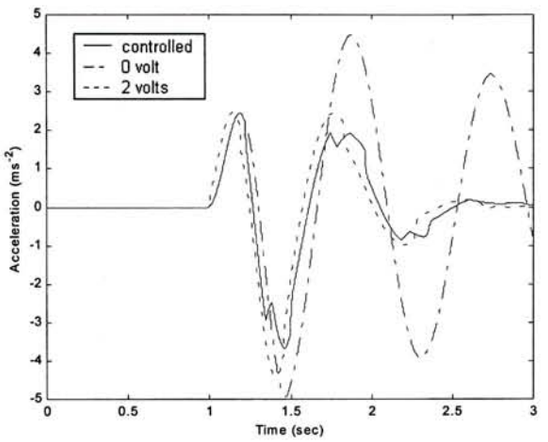


(a) Acceleration of the sprung mass (b) Displacement of the sprung mass

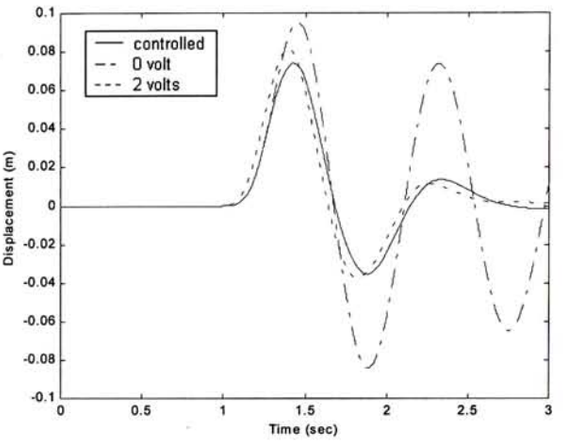
Figure 4.4: System responses under bump input using active control (with perturbation)

It is generally known that the acceleration and displacement of sprung mass are used to evaluate the performance of a suspension system. The responses of the suspension system with different controllers due to the bump excitation at the velocity of 1 m/s are shown in Figures 4.4 – 4.6. Figure 4.4 presents the excellent isolation of the system in the presence of perturbation if the MR damper can generate arbitrary force according to the sliding mode controller, i.e., the system changes from semi-active to active one. It proves the effectiveness of the sliding mode controller in the vibration suppression. So, if the controlled force can be tracked accurately, the performance of the controlled system will be good. In the latter two figures, the real cases are considered.

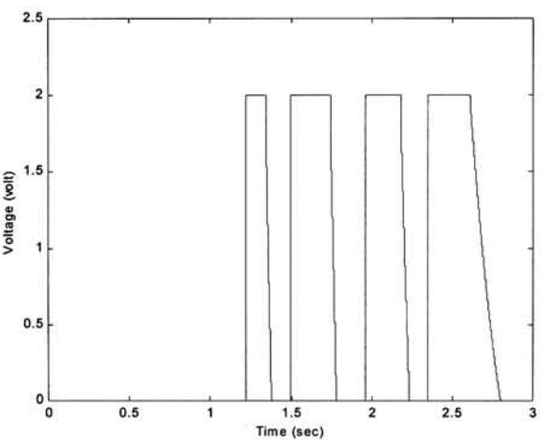
Figure 4.5 shows the results of the semi-active control action when the sprung mass is equal to the nominal mass, i.e., no mass uncertainty in the system. Figure 4.6 shows the results of the simulations in the presence of the parameter perturbation. Also, the voltages applied and corresponding damping force are shown in the figures.



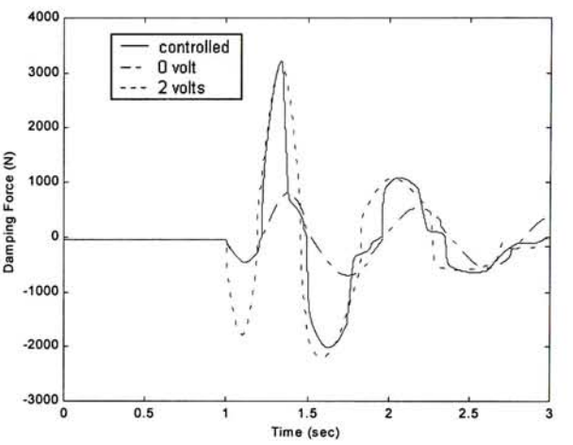
(a) Acceleration of the sprung mass



(b) Displacement of the sprung mass



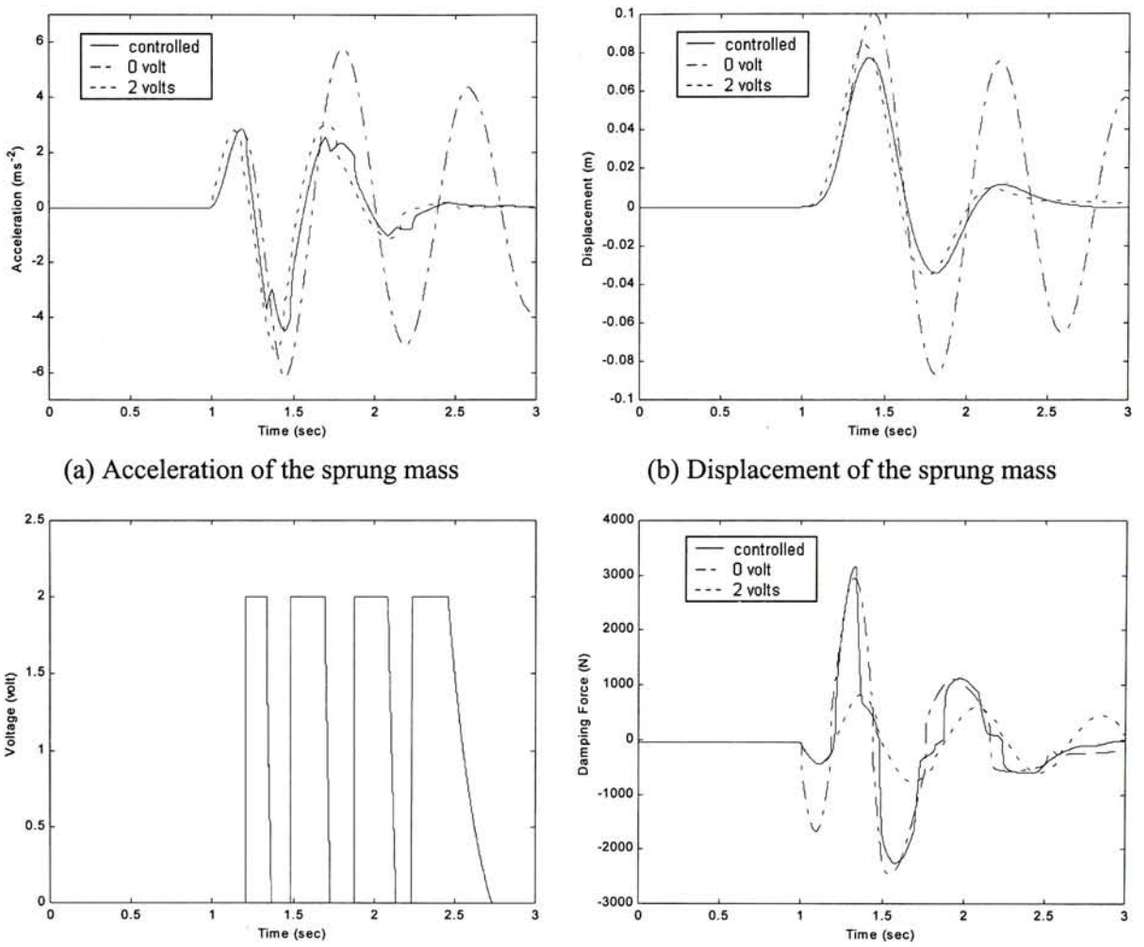
(c) Controlled voltage applied to the damper



(d) Damping force

Figure 4.5: System responses under bump input (without perturbation)

It can be seen that the acceleration of sprung mass and its displacement are reduced by employing the control voltage input determined from the sliding mode controller without and with perturbation. Constant voltage (0 and 2 volts) are applied to the damper as uncontrolled damper to be compared. The applied voltage to the MR damper is constrained to be between 0 and 2 volts. The results show that vibration suppression is not necessarily good for constant voltage input. From Figures 4.5(c) and 4.6(c), voltage is not frequently applied to the damper. Thus, obviously, the power requirement for the controlled system is much less than that for the system with constant 2 volts supply.



(a) Acceleration of the sprung mass

(b) Displacement of the sprung mass

(c) Controlled voltage applied to the damper

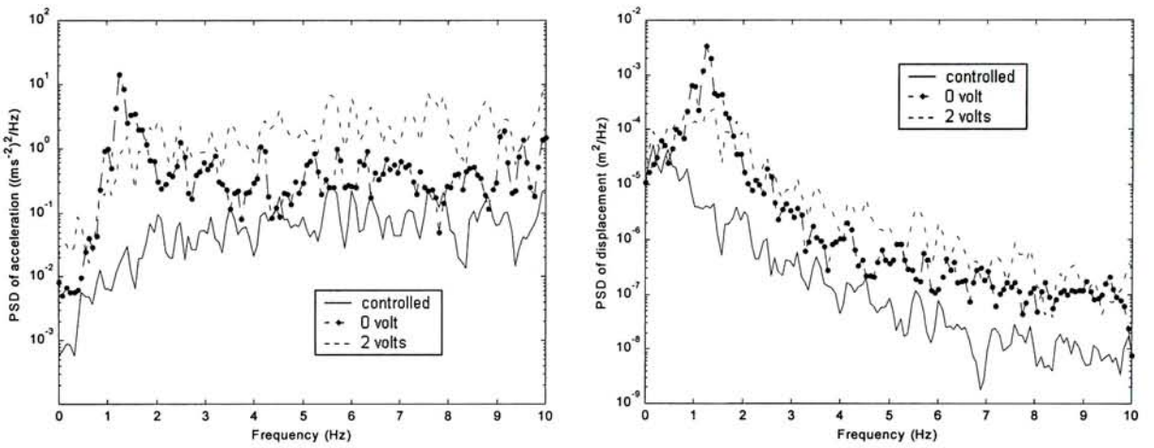
(d) Damping force

Figure 4.6: System responses under bump input (with perturbation)

4.2.2 Random Input

Similarly, the responses of the suspension system with different controllers under random excitation are shown in Figures 4.7 – 4.9. The power spectrum densities (PSD) of the displacement and acceleration of the sprung mass are presented in these figures. The frequencies most uncomfortable to humans, and therefore, those that we are concerned for PSD, are in the 0.5 Hz – 10 Hz range [36]. The resonance frequencies of the system without and with perturbation are 1.125 Hz and 1.258 Hz, respectively. Figure 4.7 presents the excellent isolation of the system using sliding mode control if the

MR damper is modeled as a force generator. It can be seen that the amplitude of the PSD is much lower than other constant voltage cases. It proves again that this robust control can work well under random excitation with mass uncertainty.

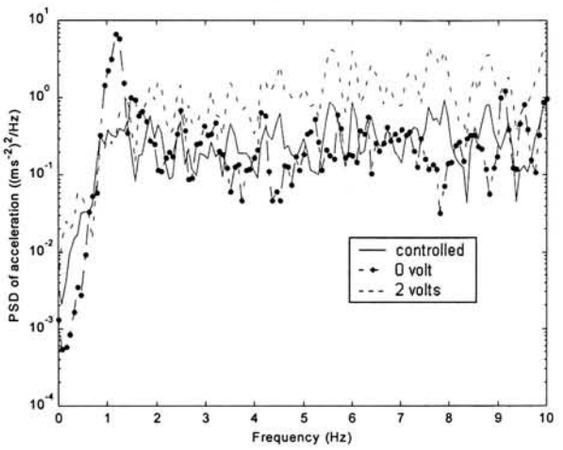


(a) Power spectral density of acceleration (b) Power spectral density of displacement

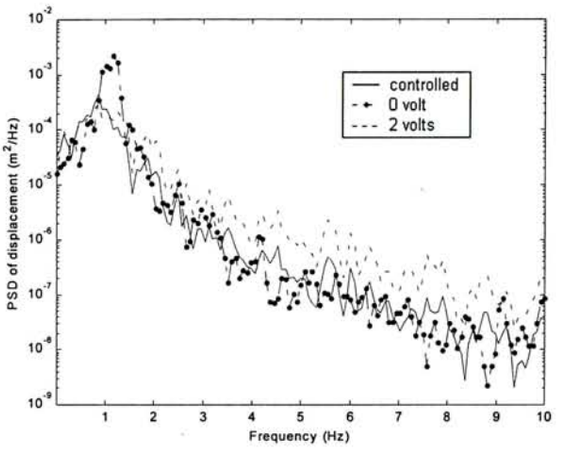
Figure 4.7: Frequency responses under random input using active control (with perturbation)

Figure 4.8 and Figure 4.9 show the performance of the controlled systems without and with uncertainty. The corresponding applied voltages and damping forces are shown in (c), (d) of Figure 4.8 and Figure 4.9. In these figures, using the controlled MR damper, the power spectral densities of displacement and acceleration of the sprung mass are significantly reduced near the resonance frequency no matter there is mass uncertainty or not.

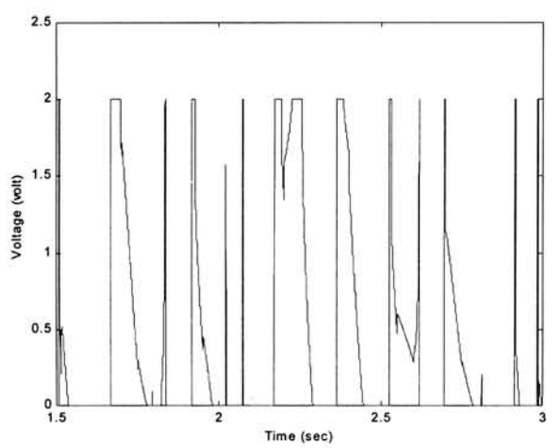
Consider the frequency from 0 to 5 Hz, the root-mean-square (RMS) values of the responses are presented in Table 4.1. Also, the average power requirement by the damper for each case is listed in that table. It should be noted that the controlled system requires much less power, compared with the system with constant 2 volts to MR damper. That particularly demonstrates the advantage of semi-active system that less power is needed while achieving better performance in vibration suppression.



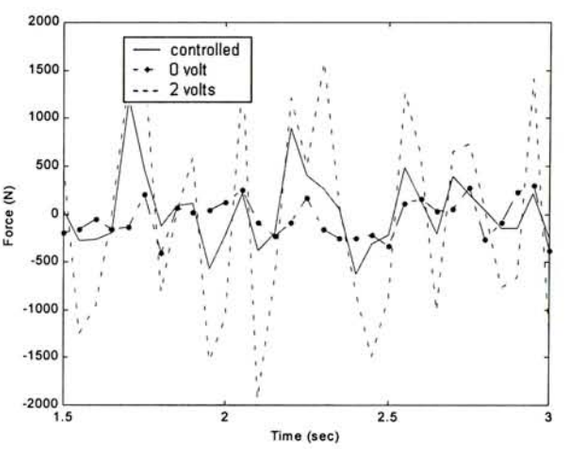
(a) Power spectral density of acceleration



(b) Power spectral density of displacement

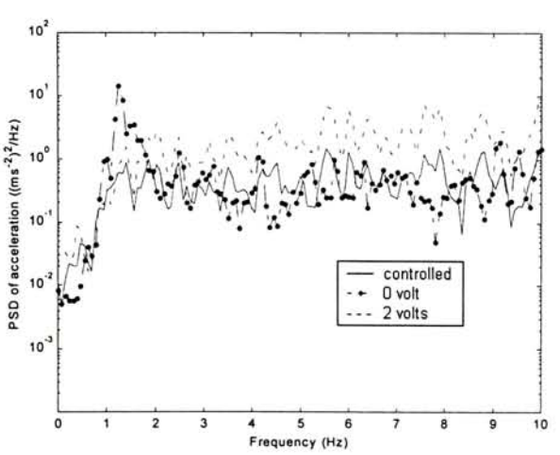


(c) Controlled voltage applied to the damper

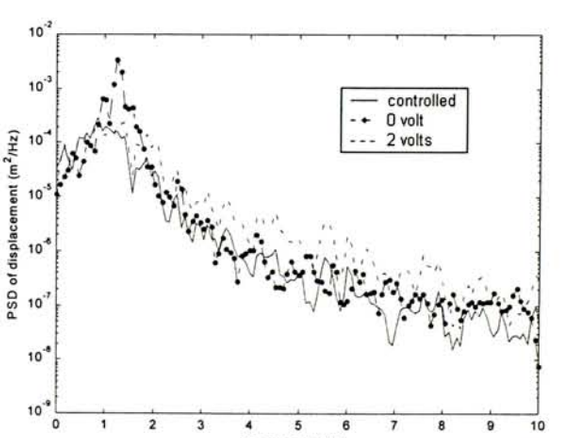


(d) Damping force

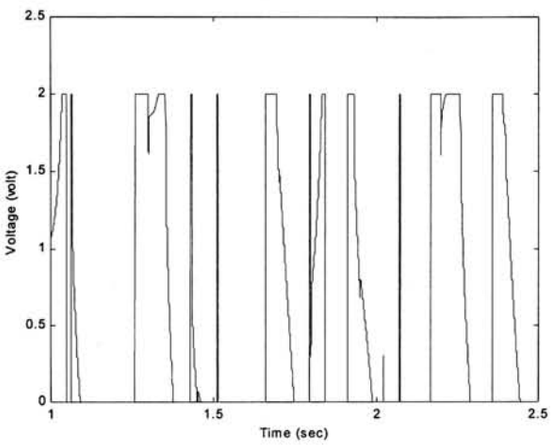
Figure 4.8: Frequency responses under random input (without perturbation)



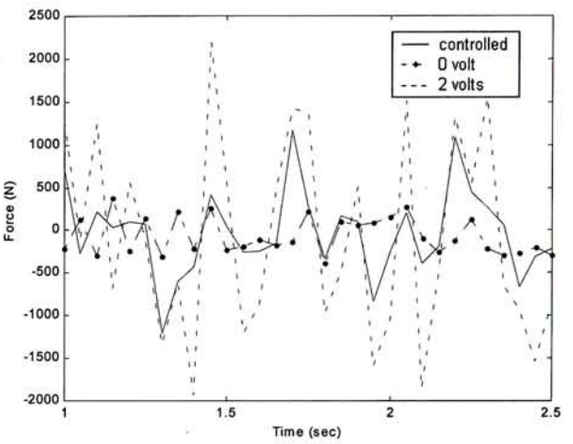
(a) Power spectral density of acceleration



(b) Power spectral density of displacement



(c) Controlled voltage applied to the damper



(d) Damping force

Figure 4.9: Frequency responses under random input (with perturbation)

Observing Figure 4.8(a) and Figure 4.9(a), the 0 volt case has a higher peak than that for the 2 volt case near the resonance frequency for the PSD of the acceleration. However, the response for 0 volt case is much lower than that for 2 volt case for higher frequencies.

Table 4.1: Comparison under random excitation

	RMS values of acceleration (ms^{-2})	RMS values of displacement (m)	Average power consumption (W)
With mass uncertainty			
Active	0.2083	0.0023	-----
Without mass uncertainty			
0 volt	0.9637	0.013	0
2 volts	1.0600	0.0073	10
With control	0.6012	0.0066	0.4321
With mass uncertainty			
0 volt	0.7321	0.0122	0
2 volts	0.8589	0.0071	10
With control	0.4781	0.0067	0.4198

Thus, the RMS values of acceleration for two uncontrolled systems are relatively close shown in Table 4.1. This characteristics has been discussed in the previous chapter by talking about the transmissibility of the passive SDOF system. On the other hand, it is shown in Figure 4.8(b) and Figure 4.9(b) that the RMS of displacement is dominated by the response near resonance frequency. The 0 volt case has the highest peak around the resonance, so the RMS value is much higher than the 2 volt and controlled cases, as shown in Table 4.1.

CHAPTER FIVE

CONCLUSION

5.1 Summary

The application of a MR fluid damper for the vibration control of a single-degree-of-freedom suspension system is proposed and studied. Firstly, the characteristics of the MR damper are investigated. And, some experiments on the damper are done. Then, a mathematical model of MR fluid damper is adopted. The parameters for the model are successfully estimated from experimental data. The SDOF suspension system with MR damper is studied and analyzed by considering its transmissibility. Also, the transmissibilities of that system are compared with those of the system with viscous damper. The non-linearity of the system is pointed out and explained by using the equivalent damping coefficient.

For vibration control of the suspension system, a sliding mode controller is designed for the robustness of the system even in the presence of the mass uncertainty. Using this control scheme, the desired damping force can be chosen. Then, a force feedback control is used to adjust the appropriate command voltage for the MR damper. Two kinds of controllers are introduced and compared. Firstly, the performances of the controlled suspension system are discussed by using transmissibility. Secondly, they are evaluated through computer simulation under two types of road excitations. Under bump input, the acceleration and displacement of the sprung mass are substantially reduced by using a controlled MR damper compared to the passive system. Under

random excitation, the ability of the MR fluid damper to reduce both peak and root-mean-square amplitudes is also shown. It should be noted that the power required for improving performance of the controlled suspension system is much lower than that of the case with constant voltages to the MR damper.

5.2 Future Work

The field test can be performed in the near future in order to investigate the effectiveness and limitations of MR suspension systems in the real implementation. One of the methods is to use Hardware-In-the-Loop (HIL) to overcome the limitations of the computer simulation.

The mathematical model of the MR damper used in this study is based on Bouc-Wen model. Besides this model, other nonparametric or parametric models can be proposed to model the nonlinear hysteretic characteristics of the MR damper. In this thesis, only two simple forms of MR damper controls have been studied. So, other control methods for the MR damper as the inner controllers can be developed. We desire to seek other control methods which can be incorporated into the dynamics of MR damper.

It is natural to extend the SDOF system to the multiple-degree-of-freedom (MDOF) system with MR dampers since many mechanical devices and structures cannot be modeled as SDOF systems only. Such systems are required to analyze the vibration of complicated systems such as automobiles and tall buildings.

APPENDIX

A.1 Semi-active Control with MR Damper – Main Program Listing

```
clear all
global A1 gamma b k0 k1 x0 aa ab c1a c1b c0a c0b n1 n
global u_new u_old y_old y_new z_old z_new h ydot
global m1 m2 g1 g2 k beta c
global volt1
global xdot3_div f_v volt_old div v_max
global i1 m k
global x1 x1dd v t f fd x1dot x0dot
global x1_r x1dd_r x1dot_r

ydot=0;

% damper model parameters
c0b=1.8034e+03;
c1b=3.4622e+04;
ab=3.8430e+04;
c0a=784.2000;
k0=3.6097e+03;
c1a=1.4649e+04;
k1=840.3726;
x0=0.0245;
aa=1.2441e+04;
gamma=1.3632e+05;
b=2059020;
A1=58.3068;
n=2;
n1=190;

%system parameters
v_max=2
ratio=5
m1=300*ratio;%estimated
m2=300*ratio-0.2*300*ratio;
k=15000*ratio;
c=7000*ratio;
g1=4;
g2=1;
G=[g1 g2];
beta=1.25;

%call sub-function
x1=sliding_app1;
```

A.2 Sub-program Listing (Dynamic System)

```
function x1=sliding_app1()

global A1 gamma b k0 k1 x0 aa ab c1a c1b c0a c0b n1 n
global u_new u_old y_old y_new z_old z_new h ydot
global m1 m2 g1 g2 k beta c
global volt1
global xdot3_div f_v volt_old div v_max
global i1 m k
global x1 x1dd v t f fd x1dot x0dot
global x1_r x1dd_r x1dot_r

%production of the excitation
freq=0.6
division=1000*2
delta_t=1/division;
h=delta_t;
V=1;
delta_x=V*delta_t;
road_length=10;
x=0:delta_x:road_length;
t=0:delta_t:road_length/V;
Amp=0.01;
base=Amp*sin(2*pi*freq*t);
x0dot1_a=V*diff(base)./diff(t);
x0dot=[0 x0dot1_a];

%%step 1
v(1)=0;
x1(1)=0;
x1dot(1)=0;

%reference
x1_r(1)=0;
x1dot_r(1)=0;
x1dd_r(1)=0;

y(1)=-0.025;
z(1)=0;
u(1)=0;
z_old=z(1);
y_old=y(1);
u_old=u(1);
x2=x1(1);
xdot=x1dot(1);
base1=base(1);
base_vel=x0dot(1);
x_r=x1_r(1);
xdot_r=x1dot_r(1);
xdd_r=x1dd_r(1);

%call sliding mode controller to produce desired force
fd(1)=sliding_app2(x2,xdot,x_r,xdot_r,base1,base_vel,xdd_r);
v1=v(1);
```

```
%call damper model to produce damping force
f(1)=sliding4_a(x2,xdot,v1,base1,base_vel);

f_p=f(1);
fd_p=fd(1);

%parameters for damper control
para=[0.021 1];
if ((fd_p-f_p*para(2))*para(1)*sign(f_p))>v_max
      v(1)=v_max;
elseif ((fd_p-f_p*para(2))*para(1)*sign(f_p))<0
      v(1)=0;
else
      v(1)=((fd_p-f_p*para(2))*para(1)*sign(f_p));
end

z(2)=z_new;
y(2)=y_new;
u(2)=u_new;
x1dd(1)=1/m2*(-k*(x1(1)-base(1))-f(1)+k1*(-0.025-x0));

%%step 2
z_old=z(2);
y_old=y(2);
u_old=u(2);
x2=x1(1);
xdot=x1dot(1);
base1=base(2);
base_vel=x0dot(2);
x_r=x1_r(1);
xdot_r=x1dot_r(1);
xdd_r=x1dd_r(1);
fd(2)=sliding4_b(x2,xdot,x_r,xdot_r,base1,base_vel,xdd_r);
f(2)=sliding4_a(x2,xdot,v1,base1,base_vel);
f_p=f(2);
fd_p=fd(2);

if ((fd_p-f_p*para(2))*para(1)*sign(f_p))>v_max
      v(2)=v_max;
elseif ((fd_p-f_p*para(2))*para(1)*sign(f_p))<0
      v(2)=0;
else
      v(2)=((fd_p-f_p*para(2))*para(1)*sign(f_p));
end

v1=v(2);
z(3)=z_new;
y(3)=y_new
u(3)=u_new;

x1dd(2)=1/m2*(-k*(x1(1)-base(1))-f(2)+k1*(-0.025-x0));
x1dot(2)=x1dd(2)*delta_t/2;
x1(2)=x1dot(2)*delta_t/3;

%reference
x1dd_r(2)=6*(k*base(2))/(6*m1+k*delta_t^2+3*c*delta_t);
```

```
x1dot_r(2)=x1dd_r(2)*delta_t/2;
x1_r(2)=x1dot_r(2)*delta_t/3;

for i=3:length(base)
   v1=v(i-1);
   x1(i)=x1dd(i-1)*(delta_t)^2+2*x1(i-1)-x1(i-2);
   x1dot(i)=(3*x1(i)-4*x1(i-1)+x1(i-2))/2/delta_t;

   x1_r(i)=x1dd_r(i-1)*(delta_t)^2+2*x1_r(i-1)-x1_r(i-2);
   x1dot_r(i)=(3*x1_r(i)-4*x1_r(i-1)+x1_r(i-2))/2/delta_t;

   base1=base(i);
   base_vel=x0dot(i);
   x2=x1(i);
   xdot=x1dot(i);
   x_r=x1_r(i);
   xdot_r=x1dot_r(i);
   x1dd_r(i)=1/m1*(-k*(x1_r(i)-base(i))-c*x1dot_r(i));
   xdd_r=x1dd_r(i);

   %sliding mode control
   fd(i)=sliding4_b(x2,xdot,x_r,xdot_r,base1,base_vel,xdd_r);
   z_old=z(i);
   y_old=y(i);
   u_old=u(i);

   %damper model
   f(i)=sliding4_a(x2,xdot,v1,base1,base_vel);
   f_p=f(i);
   fd_p=fd(i);

   %damper control to producet voltage
   if ((fd_p-f_p*para(2))*para(1)*sign(f_p))>v_max
      v(i)=v_max;
   elseif ((fd_p-f_p*para(2))*para(1)*sign(f_p))<0
      v(i)=0;
   else
      v(i)=((fd_p-f_p*para(2))*para(1)*sign(f_p));
   end

   x1dd(i)=1/m2*(-k*(x1(i)-base(i))-f(i)+k1*(-0.025-x0));
   z(i+1)=z_new;
   y(i+1)=y_new;
   u(i+1)=u_new;
end

figure
plot(t,x1);
hold on
plot(t,base,'r')
drawnow
grid
figure
plot(t,x1dd);
hold on
plot(t,base,'r')
```

A.3 Sub-program Listing (Sliding Mode Controller)

```
function force=sliding_app2(x,xdot,x_r,xdot_r,xb,xbdot,xdd_r)
global m1 m2 g1 g2 k beta x0 k1
ueq=k/m1*g2*x-g1*(xdot-xdot_r)-k/m1*xb+xdd_r;

%sliding surface
S=g1*(x-x_r)+g2*(xdot-xdot_r);
if S>= 1;
   sgn=1;
elseif S<=-1;
   sgn=-1;
else
   sgn=S;
end
un=beta*(10*abs(x)+(1-1/beta)*abs(ueq)+2+10*abs(xb))*sgn;
force=-m1/g2*(ueq-un);
```

A.4 Sub-program Listing (MR Damper Model)

```
function force=sliding_app3(xx,xdot,volt,xb,xbdot)

global A1 gamma b k0 k1 x0 aa ab c1a c1b c0a c0b n1 n
global u_new u_old y_old y_new z_old z_new h ydot

xx=xx-0.025;
%Runge-Kutta method
%u
mn1=-n1.*(u_old-volt);
mn2=-n1.*((u_old+h/2*mn1)-volt);
mn3=-n1.*((u_old+h/2*mn2)-volt);
mn4=-n1.*((u_old+h*mn3)-volt);

%y,z
kn1=1/(c0a+c0b*u_old+c1a+c1b*u_old)*((aa+ab*u_old)*(z_old-
xb)+(c0a+c0b*u_old)*(xdot-xbdot)+k0*(xx-y_old))+xbdot;

pdot2=ydot;
ln1=-gamma*abs(xdot-pdot2)*abs(z_old-xb)^(n-1)*(z_old-xb) ...
           -b*(xdot-pdot2)*abs(z_old-xb)^n+A1*(xdot-pdot2)+xbdot;
kn2=1/(c0a+c0b*(u_old+h/2*mn1)+c1a+c1b*(u_old+h/2*mn1))* ...
         ((aa+ab*(u_old+h/2*mn1))*(z_old+h/2*ln1-
xb)+(c0a+c0b*(u_old+h/2*mn1))*(xdot-xbdot)+k0*((xx-xb)-
((y_old+h/2*kn1)-xb)))+xbdot;

ln2=-gamma*abs((xdot-xbdot)-(pdot2-xbdot)).*abs(z_old+h/2*ln1-xb)^(n-
1).*(z_old+h/2*ln1-xb)-b*((xdot-xbdot)-(pdot2-
bdot)).*abs(z_old+h/2*ln1-xb)^n+A1*((xdot-xbdot)-(pdot2-xbdot))+xbdot;

kn3=1/(c0a+c0b*(u_old+h/2*mn2)+c1a+c1b*(u_old+h/2*mn2))*((aa+ab*(u_old+
h/2*mn2))*(z_old+h/2*ln2-xb)+(c0a+c0b*(u_old+h/2*mn2))*(xdot-
xbdot)+k0*((xx-xb)-((y_old+h/2*kn2)-xb)))+xbdot;
```

```
ln3=-gamma*abs((xdot-xbdot)-(pdot2-xbdot)).*abs(z_old+h/2*ln2-xb)^(n-
1).*(z_old+h/2*ln2-xb)-b*((xdot-xbdot)-(pdot2-
bdot)).*abs(z_old+h/2*ln2-xb)^n+A1*((xdot-xbdot)-(pdot2-xbdot))+xbdot;

kn4=1/(c0a+c0b*(u_old+h*mn3)+c1a+c1b*(u_old+h*mn3))*((aa+ab*(u_old+h*mn
3))*(z_old+h*ln3-xb)+(c0a+c0b*(u_old+h*mn3))*(xdot-xbdot)+k0*((xx-xb)-
((y_old+h*kn3)-xb)))+xbdot;

ln4=-gamma*abs((xdot-xbdot)-(pdot2-xbdot)).*abs(z_old+h*ln3-xb)^(n-
1).*(z_old+h*ln3-xb)-b*((xdot-xbdot)-(pdot2-xbdot)).*abs(z_old+h*ln3-
xb)^n+A1*((xdot-xbdot)-(pdot2-xbdot))+xbdot;

u_new=u_old+h/6*(mn1+2*mn2+2*mn3+mn4);
y_new=y_old+h/6*(kn1+2*kn2+2*kn3+kn4);
z_new=z_old+h/6*(ln1+2*ln2+2*ln3+ln4);
ydot=1./(c0a+c0b*u_new+c1a+c1b*u_new).*((aa+ab*u_new).*(z_new-xb)+ ...
      (c0a+c0b*u_new).*(xdot-xbdot)+k0*(xx-y_new))+xbdot;

force=(c1a+c1b*u_new).*(ydot-xbdot)+k1*(xx-x0);
```

BIBLIOGRAPHY

[1] A. H. Nizar, A. Bajwa, and D. S. Joo, "Computer controlled individual semi-active suspension system", *Proceedings of the 36th Midwest Symposium on Circuits and Systems*, Vol. 1, pp. 208-211, 1993.

[2] W. Taniwangsa and J. M. Kelly, "Experimental testing of a semi-active control scheme for vibration suppression", *Proceedings of SPIE Conference on Smart Structures and Materials: Passive Damping and Isolation*, SPIE Vol. 3045, pp. 130-139, 1997.

[3] F. Sadek and B. Mohraz, "Semiactive control algorithms for structures with variable dampers", *Journal of Engineering Mechanics*, Vol. 124(9), pp. 981-990, 1998.

[4] J. D. Carlson and K. D. Weiss, "A growing attraction to magnetic fluids", *Machine Design*, pp. 61-64, 1994.

[5] J. D. Carlson, D. M. Catanzarite, and K. A. St. Clair, "Commercial magnetorheological fluid devices", *International Journal of Modern Physics B*, Vol. 10, No. 23-24, pp. 2857-2865, 1996.

[6] S. J. Dyke, B. F. Spencer Jr., M. K. Sain, and J. D. Carlson, "Modelling and control of magnetorheological dampers for seismic response reduction", *Smart Materials and Structures*, Vol. 5, pp. 565-575, 1996.

[7] T. G. Lazareva and I. G. Shitik, "Magnetic and magnetorheological properties of flowable compositions based on barium and strontium ferrites and iron oxide", *Proceedings of SPIE Conference on Smart Structures and Materials: Passive Damping and Isolation*, SPIE Vol. 3045, pp. 185-189, 1997.

[8] O. Ashour, D. Kinder, V. Giurgiutiu, and C. Roger, "Manufacturing and characterization of magnetorheological fluids", *Proceedings of SPIE Conference on Smart Structures and Materials: Smart Materials Technologies*, SPIE Vol. 3040, pp. 174-184, 1997.

[9] O. Ashour, C. A. Rogers, and W. Kordonsky, "Magnetorheological fluids: materials characterization, and devices", *Journal of Intelligent Material Systems and Structures*, Vol. 7, pp. 123-130, 1996.

[10] W. Kordonsky, "Elements and devices based on magnetorheological effect", *Journal of Intelligent Materials, Systems and Structures*, Vol. 4, pp. 65-69, 1993.

[11] R. Bolter and H. Janocha, "Design rules for MR fluid actuators in different working modes", *Proceedings of SPIE Conference on Smart Structures and Materials: Passive Damping and Isolation*, SPIE Vol. 3045, pp. 148-159, 1997.

[12] W. H. Li, G. Z. Yao, G. Chen, S. H. Yeo, and F. F. Yap, "Testing and steady state modeling of a linear MR damper under sinusoidal loading", *Smart Materials and Structures*, Vol. 9, pp. 95-102, 2000.

[13] P. Li, G. M. Kamath, and N. M. Wereley, "Dynamic characterization and analysis of magnetorheological damper behavior", *Proceedings of SPIE Conference on Smart Structures and Materials: Passive Damping and Isolation*, SPIE Vol. 3327, pp. 284-302, 1998.

[14] C. C. Chang and P. Roschke, "Neural network modeling of a magnetorheological damper", *Journal of Intelligent Material Systems and Structures*, Vol. 9, pp. 755-764, 1998.

[15] J. Lieh, "Semiactive damping control of vibrations in automobiles", *Journal of Vibration and Acoustics*, Vol. 115(3), pp. 340-343, 1993.

[16] H. D. Taghirad and E. Esmailzadeh, "Automobile passenger comfort assured through LQG/LQR active suspension", *Journal of Vibration and Control*, Vol. 4, pp. 603-618, 1998.

[17] D. L. Margolis, "The response of active and semiactive suspensions to realistic feedback signals", *Vehicle System Dynamics*, Vol. 11, No. 5-6, pp. 267-282, 1982.

[18] S. Hwang, S. Heo, H. Kim, and K. Lee, "Vehicle dynamic analysis and evaluation of continuously controlled semiactive suspensions using hardware-in-the-loop simulation", *Vehicle System Dynamics*, Vol. 27, No. 5-6, pp. 423-434, 1997.

[19] L. R. Miller, "Tuning passive, semi-active, and fully-active suspension systems", *Proceedings of the 27th IEEE Conference on Decision and Control*, Vol. 3, pp. 2047-2053, 1988.

[20] X. Wu and M. J. Griffin, "A semi-active control policy to reduce the occurrence and severity of end-stop impacts in a suspension seat with an electrorheological fluid damper", *Journal of Sound and Vibration*, Vol. 203(5), pp. 781-793, 1997.

[21] S. B. Choi, B. K. Lee, M. H. Nam, and C. C. Cheong, "Vibration control of a MR seat damper for commercial vehicles", *Proceedings of SPIE Conference on Smart Structures and Materials: Smart Structures and Integrated Systems*, SPIE Vol. 3985, 2000.

[22] D. Karnopp, "Active and semiactive vibration isolation", *Journal of Vibration and Acoustics*, Vol. 117(3), pp. 177-185, 1995.

[23] D. Cebon, F. H. Besinger, and D. J. Cole, "Control strategies for semiactive lorry suspensions", *Proceedings of the Institution of Mechanical Engineers*, Part D, Vol. 2(2), pp. 161-178, 1996.

[24] M. Satoh, N. Fukushima, Y. Akatsu, I. Fujimura, and K. Fukuyama, "An active suspension employing an electrohydraulic pressure control system", *Proceedings of the 29th IEEE Conference on Decision and Control*, Vol. 4, pp. 2226-2231, 1990.

[25] N. Yagiz, V. Ozbulur, N. Inanc, and A. Derdiyok, "Sliding modes control of active suspensions", *Proceedings of the 12th IEEE International Symposium on Intelligent Control*, pp. 349-353, 1997.

[26] B. Mohan and S. B. Phadke, "Variable structure active suspension system", *Proceedings of the 1996 IEEE IECON 22nd International Conference on Industrial Electronics, Control, and Instrumentation*, Vol. 3, pp. 1945-1948, 1996.

[27] A. Titli, S. Roukieh, and E. Dayre, "Three control approaches for the design of car semi-active suspension", *Proceedings of the 32nd IEEE Conference on Decision and Control*, Vol. 3, pp. 2962-2963, 1993.

[28] Y. S. Kim, K. W. Wang, and H. S. Lee, "Feedback control of ER-fluid-based structures for vibration suppression", *Smart Materials and Structures*, Vol. 1, pp. 139-145, 1992.

[29] J. Y. Hung, W. B. Gao, and J. C. Hung, "Variable structure control: a survey", *IEEE Transactions on Industrial Electronics*, Vol. 40(1), pp. 2-22, 1993.

[30] R. A. Decarlo, S. H. Zak, and G. P. Matthews, "Variable structure control of nonlinear multivariable systems: a tutorial", *Proceedings of the IEEE*, Vol. 76(3), pp. 212-232, 1988.

[31] B. F. Spencer Jr., S. J. Dyke, M. K. Sain, and J. D. Carlson, "Phenomenological model of a magnetorheological damper", *ASCE Journal of Engineering Mechanics*, Vol. 123, pp. 230-238, 1997.

[32] Y. K. Wen, "Method for random vibration of hysteretic systems", *ASCE Journal of the Engineering Mechanics Division*, Vol. 102, No. EM2, pp. 249-263, 1976.

[33] M. Ahmadian, "On the isolation properties of semiactive dampers", *Journal of Vibration and Control*, Vol. 5, pp. 217-232, 1999.

[34] J.-J. E. Slotine and W. Li, *Applied Nonlinear Control*, pp. 276-310, Prentice-Hall, New Jersey, 1991.

[35] N. D. Sims, R. Stanway, A. R. Johnson, D. J. Peel, and W. A. Bullough, "Feedback control of an electrorheological long-stroke vibration damper", *Proceedings of SPIE Conference on Smart Structures and Materials: Passive Damping and Isolation*, SPIE Vol. 3672, pp. 73-81, 1999.

[36] P. Barak, "Magic numbers in design of suspension for passenger cars", *SAE Technical Papers Series*, No. 878, pp. 53-88, 1991.

CUHK Libraries
003803579